

**Synthesis of a Fully-Integrated Digital Signal Source for Communications from  
Chaotic Dynamics-based Oscillations**

by

Chance M. Glenn, Sr.

A dissertation submitted to Johns Hopkins University in conformity with the  
requirements for the degree of Doctor of Philosophy

Baltimore, MD

January 2003

© Chance M. Glenn, Sr. 2003

All Rights Reserved

## ABSTRACT

This work is the conceptualization, derivation, analysis, and fabrication of a fully practical digital signal source designed from a chaotic oscillator. In it we show how a simple electronic circuit based upon the Colpitts oscillator, can be made to produce highly complex signals capable of carrying digital information. We show a direct relationship between the continuous-time chaotic oscillations produced by the circuit and the logistic map, which is discrete-time, one-dimensional map that is a fundamental paradigm for the study of chaotic systems. We demonstrate the direct encoding of binary information into the oscillations of the chaotic circuit. We demonstrate a new concept in power amplification, called *syncrodyne amplification*, which uses fundamental properties of chaotic oscillators to provide high-efficiency, high gain amplification of standard communication waveforms as well as typical chaotic oscillations. We show modeling results of this system providing nearly 60-dB power gain and 80% PAE for communications waveforms conforming to GMSK modulation. Finally we show results from a fabricated syncrodyne amplifier circuit operating at 2 MHz, providing over 40-dB power gain and 72% PAE, and propose design criteria for an 824 -850 MHz circuit utilizing heterojunction bipolar transistors (HBTs), providing the basis for microwave frequency realization.

Copyright, 2003, by Chance M. Glenn, Sr., All Rights Reserved.

This thesis is dedicated to my wife Marsha. She has undoubtedly remained by my side through every kind of weather. I would not have been able to do this without her. Even during the writing of this dissertation your importance to me is demonstrated. Also, to my God, and my Savior, Who gave my wife and my children, Michael, Markiss, Melyssa and Morgen to me, and Who inspires creativity and perseverance in all of His children,  
thank You.

## ACKNOWLEDGMENTS

I would like to acknowledge my advisor, Dr. Charles R. Westgate, for the consistent encouragement to push farther, the freedom to explore new ideas and the persistency to never let me quit.

I would also like to acknowledge Dr. Scott T. Hayes, who first became my friend, then became my mentor, then became my colleague, and finally became my business partner. Our relationship has indeed been fruitful over these 16 years. We have plenty more mountains to climb I'm certain. I could not have done this without his inspiration to never settle for mundane ideas, to explore deeper than the average, and to pursue scientific knowledge with vigor and integrity. He has helped to shape my character more than he could ever know.

I would like to acknowledge Dr. Christian Fazi, who first put this hair-brained idea in my head to pursue my Master's and Doctoral degrees. He has remained a constant source of encouragement through the ups and the downs. His contagious love for new ideas is one of the reasons I was able to stay on this course.

I would finally like to acknowledge all of my immediate family: father and mother Wallace and Shirley, my siblings: Wallace, who I grew up the closest to and gave me my sense of drive and competitiveness, Victoria, Christopher, Patty, Robin, Carlton and Cameron, who saw my love for tearing things apart to see how they worked, and steered me down the road of electronics and engineering, and finally my grandmother who raised me. I love you all.

# TABLE OF CONTENTS

	Page
LIST OF TABLES .....	vii
LIST OF FIGURES .....	viii
Chapter	
1. Introduction.....	1
1.1 Description of the Work .....	1
1.2 Chaotic Dynamics .....	3
1.3 Applications of Chaotic Dynamics.....	10
1.4 Communication and Chaotic Dynamics.....	10
1.5 Wireless Communications and the Opportunity.....	12
2. A Paradigm Study: The Colpitts Oscillator .....	16
2.1 Rationale.....	16
2.2 Properties and Measures.....	20
2.3 The Colpitts Oscillator as a Digital Signal Source.....	23
2.4 Syncrodyne Amplification.....	28
2.5 Modeling Results and Analysis .....	31
3. Custom Chaotic Oscillator Design. ....	41
3.1 Design Criteria.....	41
3.2 PSPICE Modeling .....	43
3.3 Circuit Fabrication and Testing.....	46
3.4 Preliminary Design of a 850 MHz Circuit .....	53
4. Conclusion .....	57
4.1 Discussion of Results .....	57
4.2 Implications .....	59
APPENDIXES	
A. MATLAB Procedures for Modeling and Analysis.....	61
B. SPICE Circuit Files.....	79
LITERATURE CITED .....	81
VITA.....	84

## LIST OF TABLES

Table	Page
1.1. Demonstration of the spreading of initial conditions for the logistic map for $\rho = 4$ (chaotic) .....	7
1.2. Mobile Handset Market: Mobile Subscriber Forecast (World), 1999 – 2005 .....	12
1.3. Summary of performance parameters for the leading PA products.....	13
2.1. Calculation of local Lyapunov exponents for the discrete time mapping of the Colpitts oscillator. ....	22
2.2. Circuit parameter values used for syncrodyne amplifier model analysis .....	31

## LIST OF FIGURES

Figure	Page
1.1. Plots of the logistic map for $\rho = 1, 2, 3$ and 4.....	4
1.2. Bifurcation diagram for the logistic map as parameter $\rho$ is varied.....	6
1.3. Two chaotic oscillators synchronized together. Oscillator B tracks the identical behavior of oscillator A .....	9
1.4. Lorenz oscillations encoded to carry a digital sequence which produces the ASCII text ‘c-h-a-o-s’ .....	11
1.5. A typical I-V characteristic curve for a transistor describing the linear and nonlinear regions of operation .....	14
2.1. A general voltage feedback system.....	16
2.2. Transistor based Colpitts oscillator circuit used for this analysis.....	16
2.3. Collector voltage versus time for the Colpitts circuit using a parameter set that produces Rössler type chaos. ....	18
2.4. Three-dimensional representation of the state-space trajectories for the Colpitts oscillator illustrating the Rössler band.....	18
2.5. Power spectrum of the collector voltage for the Colpitts oscillator in a chaotic mode of operation .....	19
2.6. Chaotic attractor for the Colpitts oscillator with an Poincaré surface of section erected in the flow.....	20
2.7. Poincaré map produced by the surface of section in figure 2.6.....	21
2.8. Return map for the collector voltage as produced by sequential observation of points generated by the Poincare mapping. Note its resemblance to the logistic map.....	21
2.9. The return map for the Colpitts chaotic oscillator illustrating the binary partition and the generation of digital information.....	23
2.10. The Poincaré map of the Colpitts chaotic oscillation showing the placement of the	



binary partition boundary. Trajectories passing through the Poincaré surface of section on either side of the boundary produce bit 0 or 1 .....	24
2.11. 8-bit binary coding function for the Colpitts oscillator .....	25
2.12. State-space trajectories encoded to produce the 8-bit binary sequence 01011101. ....	26
2.13. Time-varying collector voltage demonstrating the 8-bit binary encoding 01011101 embedded into the oscillations.....	27
2.14. Block diagram of a Syncrodyne amplifier system.....	29
2.15. Circuit schematic diagram for a Colpitts oscillator based syncrodyne amplifier .	30
2.16. (a) In-phase and (b) quadrature baseband components of a 2 MHz GSM waveform along with (c) the modulated carrier and (d) the power spectrum.....	34
2.17. Variation of the attractor volume as the capacitor $C$ is changed .....	35
2.18. Power gain as a function of the tuning capacitance $C$ .....	36
2.19. Surface map illustrating the PAE for peak-to-peak input voltages and tuning capacitance values.....	37
2.20. Relationship between the peak power gain and the peak sinusoidal input voltage for the syncrodyne amplifier circuit.....	38
2.21. Overall PAE peak power gain relationship for the syncrodyne amplifier circuit. Note that there are regions of operation where the system is capable of nearly 80% PAE and greater than 55 dB gain. ....	39
3.1. 2 MHz syncrodyne amplifier circuit schematic diagram.....	42
3.2. Two-dimensional projection of the chaotic attractor produced by the 2 MHz Colpitts oscillator SPICE simulation .....	44
3.3. Time-dependent oscillation of the emitter voltage in a slightly chaotic state.....	44
3.4. Frequency spectrum of the emitter voltage oscillations illustrating the broad frequency content indicative of chaotic behavior .....	45
3.5. Photograph of the fabricated 2 MHz syncrodyne amplifier circuit .....	46
3.6. Picture of the PCB used to fabricate the 2 MHz syncrodyne amplifier circuit.....	46

3.7.	Measured time signal from the Colpitt's oscillator circuit .....	47
3.8.	The Colpitts attractor controlled on a constrained set. The Cantor set structure is a result of the constraint.....	48
3.9.	Uncontrolled 2 MHz Colpitts attractor showing a two-dimensional projection of the state-space attractor.....	49
3.10.	Symbolic dynamics controlled Colpitts attractor.....	50
3.11.	Results from the 2 MHz syncrodyne amplifier circuit showing (a) the input signal, (b) the output signal and (c) the error signal .....	51
3.12.	Comparison of experimental data from the 2 MHz syncrodyne amplifier with modeling results .....	52
3.13.	DC I-V characteristics for the high-frequency HBT used to model the 850 MHz circuit .....	53
3.14.	Schematic diagram of the high-frequency, Colpitts type, chaotic oscillator modeled using an HBT .....	54
3.15.	Time dependent oscillation of the voltage $v_{C1}$ for the 850 MHz chaotic oscillator simulation.....	55
3.16.	Two-dimensional projection of the state-space for the 850 MHz chaotic oscillator simulation.....	56
3.17.	Frequency spectrum for the voltage across $C_1$ for the 850 MHz chaotic oscillator simulation.....	56

# CHAPTER 1

## Introduction

### 1.1 Description of the Work

This work represents original concepts derived by the author and is intended to demonstrate that the engineering implementation of chaotic oscillations in digital communications systems can show clear performance enhancements as compared to traditional designs. We intend to show this in two ways. First, we intend to show that it is both possible and practical to encode arbitrary binary information into chaotic oscillations. There has been a great deal of prior formalization and experimentation surrounding the application of chaos to communications [1,2]. We show the benefits of using the direct encoding method of controlling symbolic dynamics first proposed by Hayes, et. al [3]. Second, we introduce formally and demonstrate experimentally, a new method of high-gain, high-efficiency power amplification of standard communication waveforms using a chaotic process. We show that this process, called syncrodyne amplification, is capable of operating on communication waveforms such as GSM and CDMA and capable of providing gains in excess of 60 dB and power added efficiencies greater than 70%.

In a general sense, the goal of this work is to provide further evidence of the notion that chaotic dynamics can be useful for technological applications. The paradigm shift that occurred in the dynamics community when the implications of chaotic dynamics was understood [4] has not been fully realized in applied engineering circles. A primary reason for this has been the failure to present tangible performance advantages of chaotic systems over traditional systems. Our goal is to provide solid examples of such

advantages.

## 1.2 Chaotic Dynamics

What is chaos? After over one hundred years of research, study, scrutiny, analysis, modeling, and experimentation, this is a question that still eludes a definitive answer. Chaos is better defined by its behavior or its properties. Chaos is a descriptive term for the properties of a system in motion, or a *dynamical system*. Therefore chaotic behavior is often referred to as *chaotic dynamics*. More specifically, chaotic dynamics is a type of behavior that occurs in nonlinear systems.

Most credit Henri Poincaré for being the one to begin the work around the turn of the 20<sup>th</sup> century [5]. Poincaré was a French mathematician who studied the three-body problem in orbital dynamics, considering the interaction of three celestial bodies undergoing mutual gravitational attraction. He was able to show complex, now called chaotic, orbits arising from different sets of initial conditions. Today much of the terminology used in reference to chaotic dynamics has its roots in orbital dynamics. The name *chaos* was first associated with this type of dynamics by James Yorke of the University of Maryland [6].

Chaotic dynamics appears within a whole host of scientific disciplines. As mentioned above, orbital dynamics, as well as the physics of pendulums [7], weather phenomena, predator-prey models, microwave circuits [8,9], and a myriad of other areas of science and engineering have produced chaotic dynamics either in theory or in experimentation. Again, what is chaos? Let us begin to answer this question by describing some key properties that will be important to the development of this work. These properties are (1) sensitivity to small perturbations, (2) fractal dimension, and (3) synchronization.

First let us consider a simple one-dimensional discrete-time map called the logistic map. This non-invertible map is a simplified model for an ecological balance

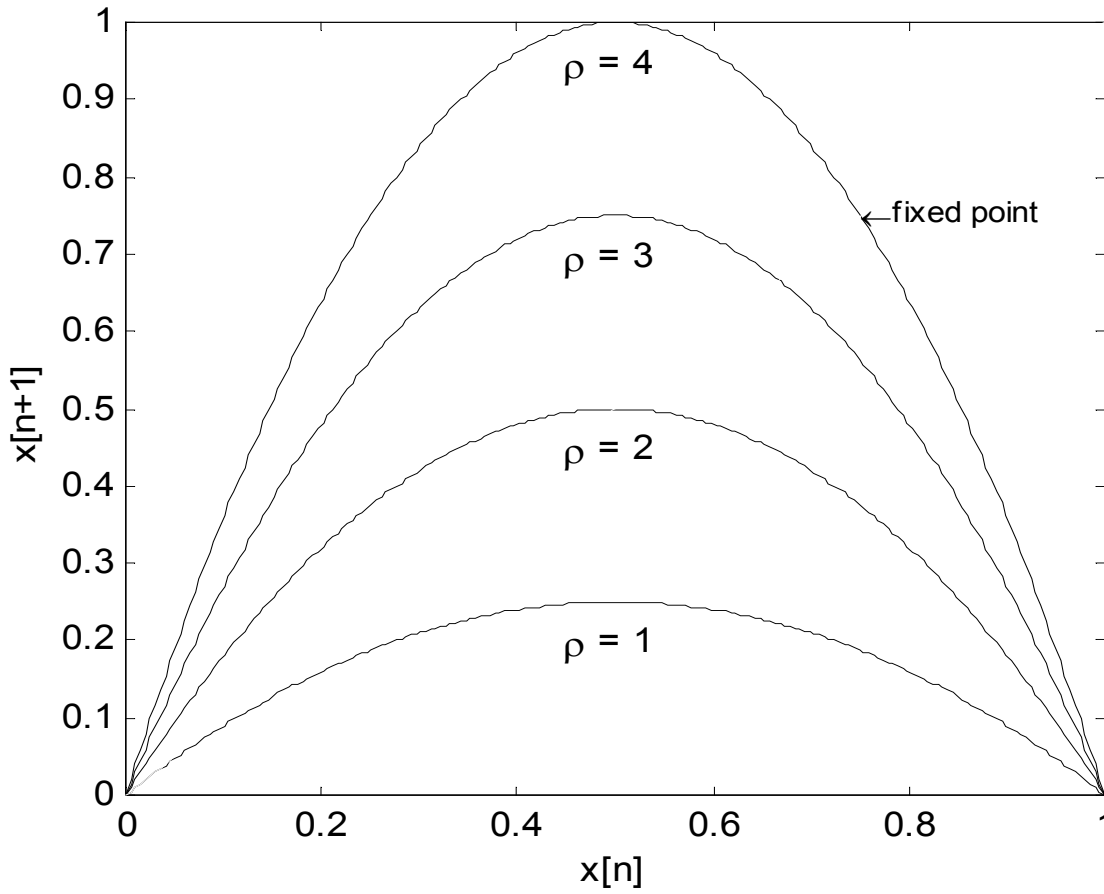


Figure 1.1 Plots of the logistic map for  $\rho = 1, 2, 3$  and 4.

such as predator-prey [10]. It is described by the expression,  $x_{n+1} = \rho x_n(1 - x_n)$ , where  $\rho$  is a parameter that takes on values ranging from 1 to 4. Figure 1.1 is a plot of this function for differing values of  $\rho$ . Let us begin to notice some of the characteristics of this map that will help us understand some of the general nature of chaotic dynamics.

It is first important to note that this map is not generally chaotic. It has regions of chaos determined by the parameter  $\rho$ . There are points of attraction, or an *attractor*, for

each parameter value. In some cases this attractor is a point, in others it is a set of points.

We start by finding the fixed point(s),  $x_p$ , letting the quadratic expression be

$y = \rho x_p (1 - x_p) = x_p$ , which yields the solution  $x_p = [0, 1 - \frac{1}{\rho}]$ . These are the values that

the map will tend towards and remain at after several iterations, regardless of the initial

conditions. Figure 1.2 shows what is commonly called a bifurcation diagram for the

logistic map. As the parameter  $\rho$  is varied, several values of  $x_n$  are collected.

When  $\rho = 3.56994\dots$  (typically referred to as  $\rho_\infty$ ), chaotic behavior occurs. Prior to that, the map undergoes a typical period-doubling route to chaos. That is, the number of non-trivial fixed points doubles over intervals specified by  $\rho$ . Mitchell Feigenbaum derived a scaling law for the onset of chaos via a period doubling route [7]. The

Feigenbaum number is described by:  $\frac{\rho_{m+1} - \rho_m}{\rho_m - \rho_{m-1}} \rightarrow 4.66920\dots$ , where  $m$  is the period

number. It has been observed in various physical experiments.

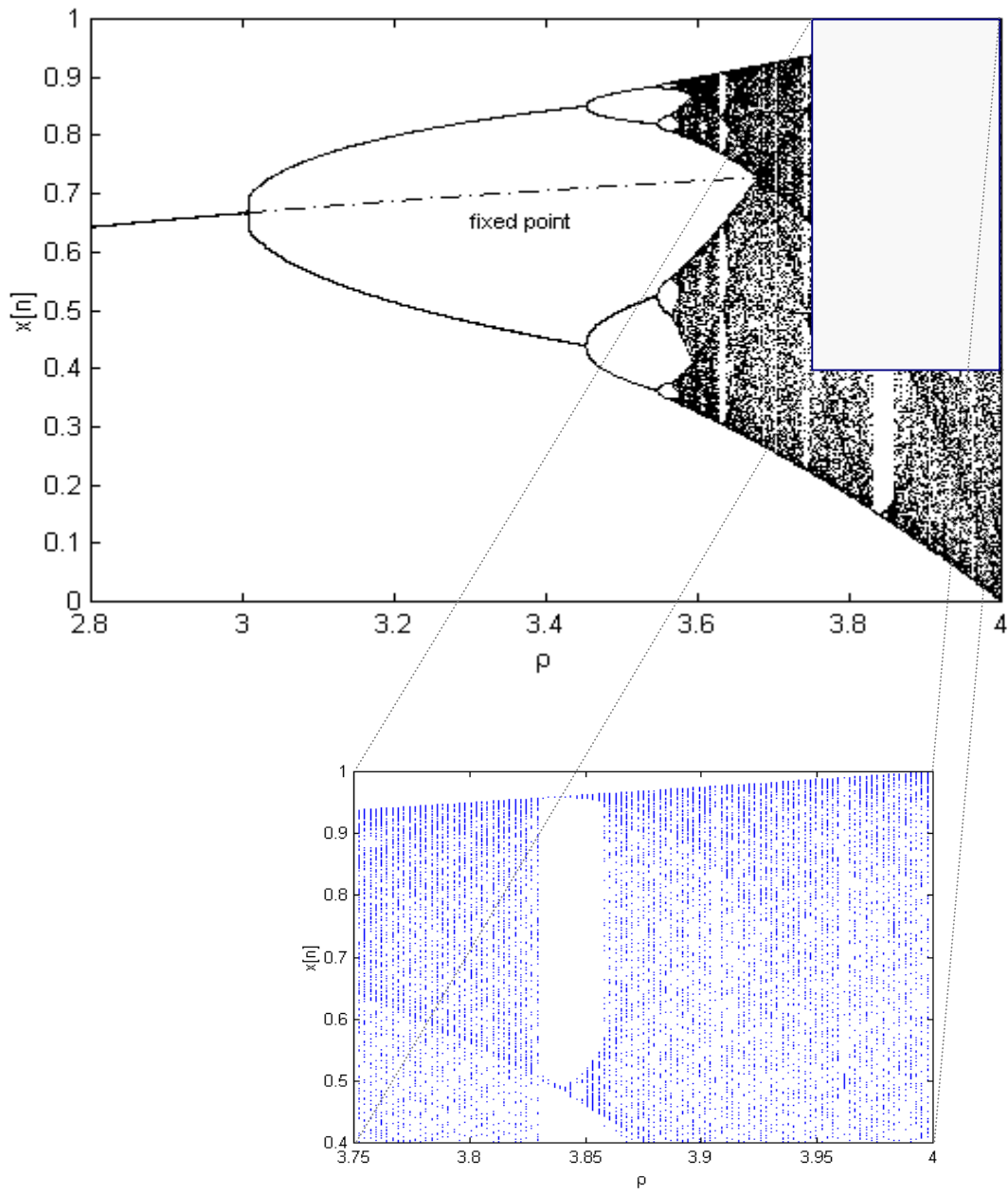


Figure 1.2 Bifurcation diagram for the logistic map as parameter  $\rho$  is varied.



One of the more noted properties of chaotic dynamics is its sensitivity to small perturbations. Often referred to as the *Butterfly Effect*, referring to the notion that a butterfly flapping its wings in China could initiate a storm in New York next month, this property is indicative of seemingly random behavior occurring in sometimes very simple systems. Chaotic systems do not produce random behavior, however, solutions become increasingly uncorrelated to its initial conditions as time increases. This is best illustrated with an example using the aforementioned logistic map. The table below shows three separate values from the map at  $\rho = 4$ , after 10 iterations, given three initial conditions separated by 0.01. Variations in the ending points are significantly greater than the variation of the initial conditions. Unless the initial condition is known with infinite precision, it becomes impossible to predict the outcome of the map for all time. The slope of the map,  $\frac{dy}{dx} = \rho - 2\rho x$ , governs the spreading of a point on the map. A true measure of the sensitivity to small changes in this chaotic map and any other chaotic system is called the *Lyapunov exponent* [7]. If we let  $d_n$  be the difference between any two points at iteration time  $n$ , the relationship  $d_n = d_0 2^{2n}$  holds, and  $\lambda$  is the Lyapunov exponent. It has been shown that the Lyapunov exponent must be positive for chaotic behavior to exist [11].

Table 1.1 Demonstration of the spreading of initial conditions for the logistic map for  $\rho = 4$  (chaotic).

$x_0$	$d_0$	$x_{10}$	$\Delta x$	$d_{10}$	$\lambda$
0.199	--	0.8160	0.6170	--	
0.200	0.001	0.9616	0.7616	0.1446	0.7176
0.201	0.002	0.4488	0.2478	0.3692	0.7528

The attractor is the point or set of points in state space that the system tends to be drawn to. For the logistic map with a parameter value greater than  $\rho_\infty$  the attractor is a set of points that are chaotic and indeed fractal, thus the attractor is referred to as a *strange attractor*. Benoit Mandelbrot coined the term fractal, where he referred to objects having *fractional dimension*. There are different types of dimension, however the Hausdorff dimension, indicated by  $D_0$ , is the physical dimension that we are most familiar with, and is often called the box-counting dimension [10]. Therefore, a chaotic system that has an attractor whose Hausdorff dimension is non-integer is said to have a strange attractor. The Hausdorff dimension of the logistic map has been calculated, for  $\rho = \rho_\infty$ , to be  $D_0 = 0.618\dots$ , which is greater than a point ( $D_0 = 0$ ), but less than a line ( $D_0 = 1$ ).

Another interesting and important property of chaotic systems is their tendency to synchronize with each other. Pecora and Carroll first reported this phenomena in chaotic circuits and has since laid the foundation for a great many applications of the synchronous behavior of chaotic circuits in practical electronics [12,13]. This property is also intimately related to the ability of chaotic oscillators to be controlled using small perturbations. This groundbreaking work was first introduced by Ott, Grebogi, and Yorke [14] and has been responsible for a flood of research, development, and applied technology in the area of chaotic dynamics. We will show how specific continuous-time chaotic systems, such as chaotic circuits, are directly related to discrete-time chaotic maps like the logistic map, and how the synchronization properties are crucial to the development of technologically beneficial applications. Figure 1.3 is an illustration of two chaotic oscillators synchronized together.

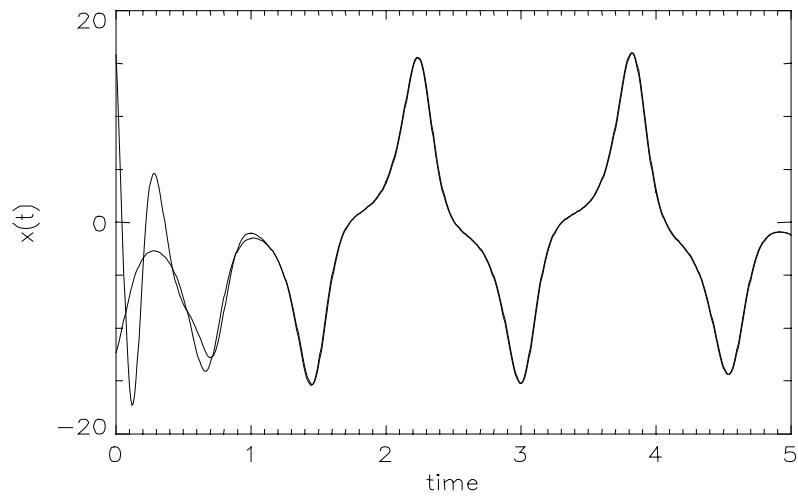
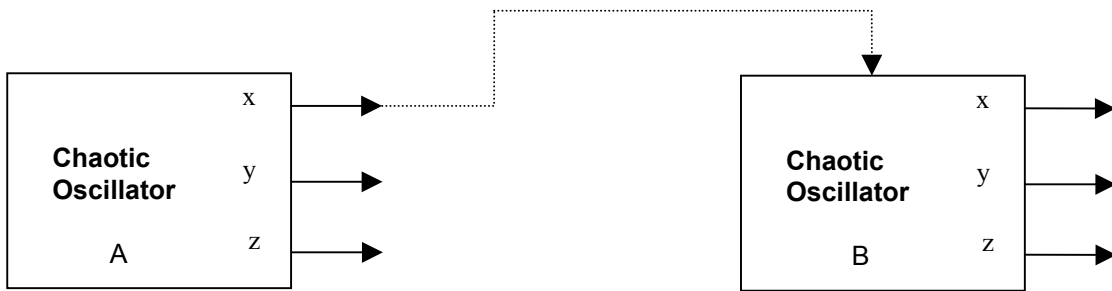


Figure 1.3 Two chaotic oscillators synchronized together. Oscillator B tracks the identical behavior of oscillator A.

### 1.3 Applications of Chaotic Dynamics

Since Ott, Grebogi and Yorke's paper in 1990 there has been a tremendous push for the application of chaotic dynamics to technology. Like other endeavors of the 90's many a student, professor and entrepreneur rushed to this area to find what gems lie there. Technology companies have been established, employing researchers in chaotic dynamics in order to find important links to commercial technology. Applications ranging from the control of fluid dynamics, weather prediction and control, spacecraft guidance, sensors and detection, and control of lasers, to various facets of communications have been studied and in some cases put into practice.

### 1.4 Communication and Chaotic Dynamics

By far, the most intriguing and sought after application of chaotic dynamics is in the area of communications. In 1993 Hayes described a formal linkage between chaotic dynamics and information theory [15], showing that the symbolic dynamics of a chaotic system could be controlled, thereby paving the way for encoding of digital information into a chaotic oscillation [16]. That has been the basis for serious engineering applications in this area. Figure 1.4 shows the oscillations of the Lorenz systems of equations encoded to produce a pre-described digital sequence.

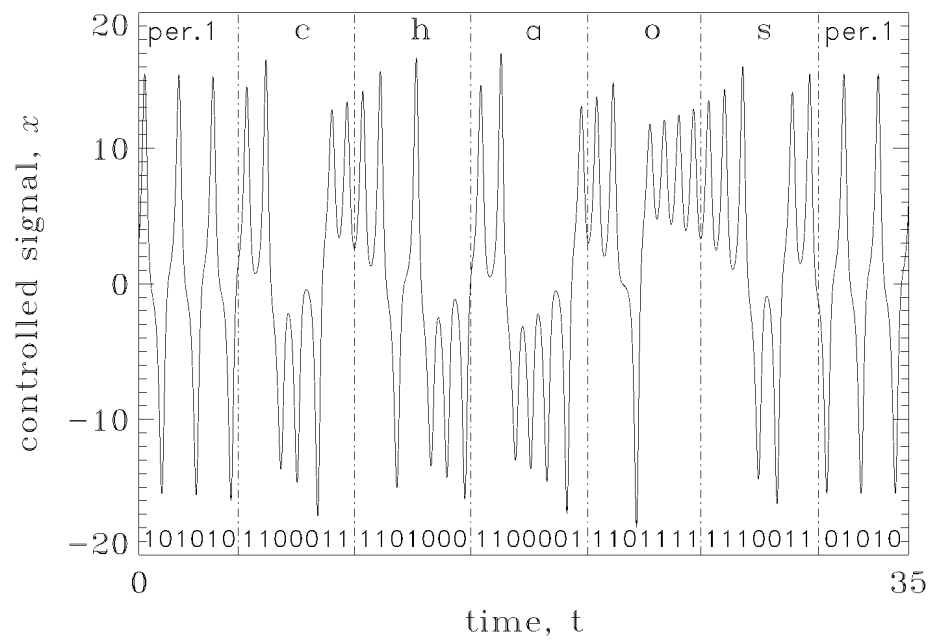


Figure 1.4 Lorenz oscillations encoded to carry a digital sequence which produces the ASCII text 'c-h-a-o-s'.

## 1.5 Wireless Communications and the Opportunity

Over the past few years the intent of effort in chaotic dynamics has moved from the arena of research to applied science, to applications engineering, to commercialization. At the same time the communications industry has squarely trained its focus on wireless technology. Even though there has been a significant down-turn in the past year or so in this industry, there still remains significant optimism as consumer demand for new features and the integration of current features continues to grow [17]. Table 1.2 below shows world mobile handset subscribers, past, present, and projected through 2005, having a compound annual growth rate of 16.5%. Regardless of the commercial climate, there is a large, ever-evolving market for wireless communications.

Table 1.2 Mobile Handset Market: Mobile Subscriber Forecast (World), 1999 – 2005.

Year	Subscribers (Million)	New Additions (Million)	Subscriber Growth Rate (%)
1999	477.5	159.5	-
2000	722.0	244.5	51.2
2001	943.3	221.3	30.7
2002	1,151.5	208.2	22.1
2003	1,363.6	212.1	18.4
2004	1,560.1	196.5	14.4
2005	1,739.0	178.9	11.5
CAGR			16.5%

CAGR = Compound Annual Growth Rate (2001-2005)

One of the greatest challenges for the mobile wireless communications industry has been the provision of mobile power sources capable of meeting the growing demand by users. Improvement and integration of features in mobile handsets increase on-time, and processor requirements, all placing higher demand on the battery. According to Frost & Sullivan, the development of battery technology, specifically its energy storage

capacity, has not kept up with the demand by the mobile wireless industry [18]. The solution to this dilemma lies in the efficient utilization of the power provided. In mobile communications the power amplifier uses the bulk of the supply power. Table 1.3 shows a survey of the leading power amplifier products and the performance of their products.

For a power amplifier, power added efficiency (PAE) is defined by  $PAE = \frac{P_o - P_{in}}{P_{dc}}$ ,

where  $P_o$  is the output power,  $P_{in}$  is the input power, and  $P_{dc}$  is the power delivered by the dc source. As shown by the table, efficiencies tend not to exceed 50% in practice. This wasted energy, often in the form of heat, is due to employment of inefficient linear design techniques in order to meet the strict spectral requirements required by the industry.

Table 1.3. Summary of performance parameters for the leading PA products.

	<b>Raytheon</b>	<b>RF Micro Devices</b>	<b>IBM</b>	<b>Sirenza</b>
Part Number	RMPA0951A-102	RF2162	2018M009	SPA-2118
Gain	30 dB	29 dB	28 dB	32.5 dB
PAE	30%/44%	35%/50%	34%/48%	38%
Harmonics	-30 dBc	-30 dBc	-30dBc	-30 dBc
Noise Figure	-	-	-	5.0 dB
3 <sup>rd</sup> Order Intercept				48.0 dB
Dynamic Range	85 dB	85 dB	85 dB	85 dB

It is well known that the operation of electronic circuits and devices in the strongly nonlinear regions yields higher power conversion efficiency [19]. The heart of chaotic dynamics is its operation in the nonlinear regions of the system. Figure 1.5 shows a typical I-V characteristic for a transistor. Traditional designers bias their circuit such that the transistor is operating in the linear region. This type of operation limits the output voltage swing of the circuit. Although the circuit may be capable of producing output voltages outside of the linear region of the transistor, the circuit is purposely

designed to avoid this. Circuits that are designed to operate in the nonlinear region of the transistor's operation are capable of broader output voltage swings and even higher current, thus capable of higher output power, thus capable of higher power conversion efficiency.

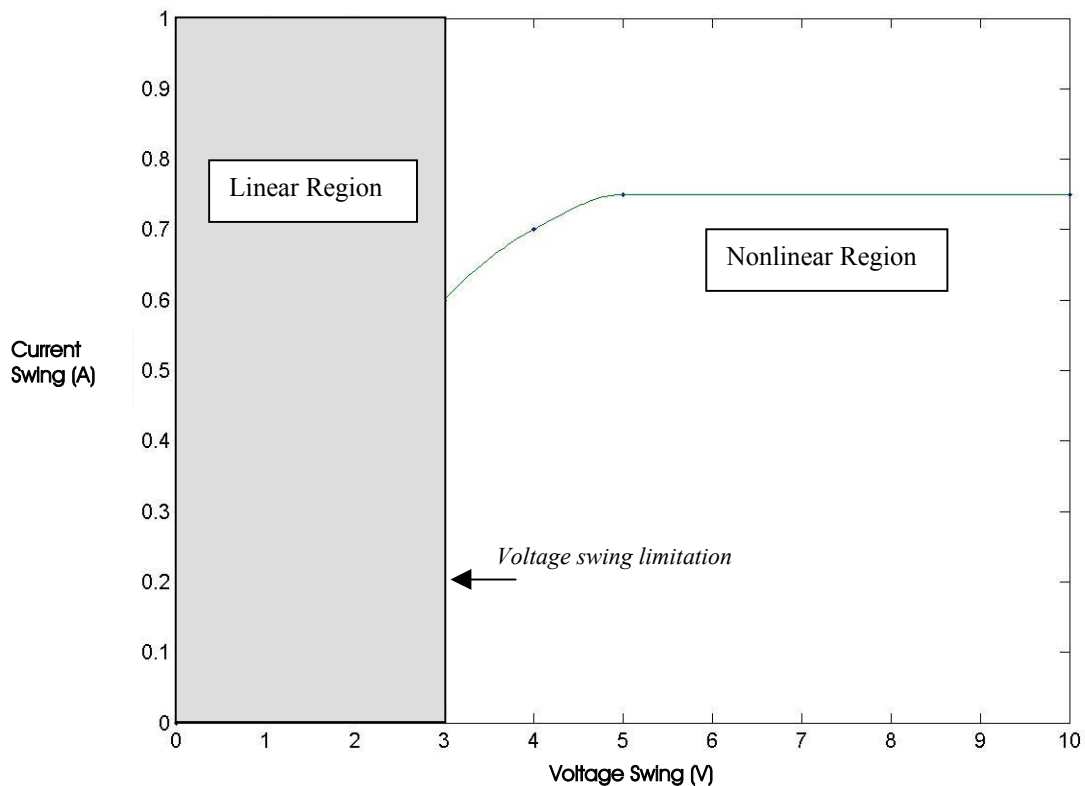


Figure 1.5 A typical I-V characteristic curve for a transistor describing the linear and nonlinear regions of operation.

Chaotic oscillations occur as a result of operating the system in its nonlinear state. This is not to say that all nonlinear operation results in chaos, only that the system must be nonlinear in order for chaos to exist. There is also a natural complexity to the oscillations of a sometime very simply realized chaotic system that makes these systems attractive for communications applications. The goal of this work is to show that



generation of chaotic signals for highly efficient amplification and transmission of digital communications waveforms for wireless telecommunications is practical, realizable, and technologically beneficial.

## CHAPTER 2

### A Paradigm Study: The Colpitts Oscillator

#### 2.1 Rationale

In this chapter we will consider the Colpitts oscillator as our chaotic oscillator of choice. There are three fundamental reasons why we choose this particular oscillator. The first reason is that the Colpitts configuration has been a staple of communications electronics for years. Most analog electronic circuits that require sinusoidal signal employ Colpitts circuits. Suppose we have the general series voltage feedback system shown in figure 2.1. The voltage gain of the amplifier section is  $A$  and the voltage transfer of the feedback section is  $\beta$ . The overall gain of the system is given by,

$$A_f = \frac{A}{1 + \beta A}. \text{ When } \beta A = -1, \text{ or has magnitude 1 at a phase angle of } 180^\circ, \text{ then oscillation}$$

will occur. This is known as the *Barkhausen criterion* [20]. The distinction of the Colpitts circuit is in the feedback portion of the circuit. Figure 2.2 is the Colpitts circuit used for this analysis. Note the feedback is a tank circuit consisting of an inductor and

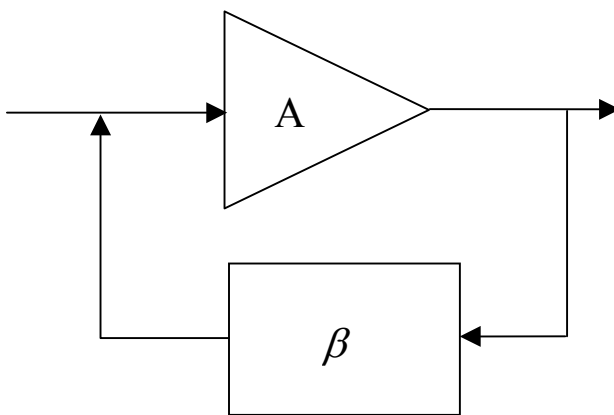


Figure 2.1 A general voltage feedback system.

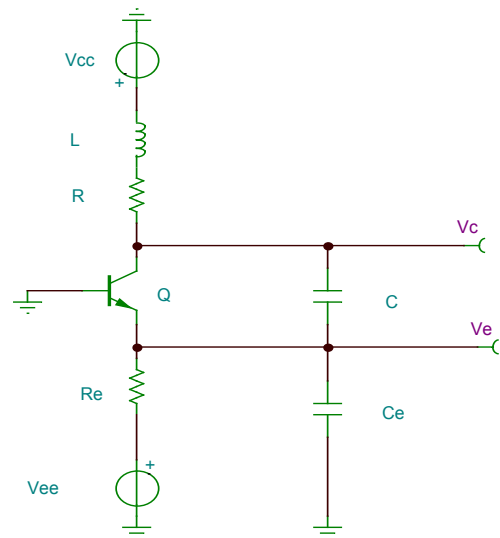


Figure 2.2 Transistor based Colpitts oscillator circuit used for this analysis.

two capacitors. The resonant frequency is given by  $\omega = \sqrt{\frac{C + C_e}{LCC_e}}$ . The circuit equations are,

$$L \frac{di_L}{dt} = V_{CC} - v_c - (R + R_L)i_L$$

$$C_e \frac{dv_e}{dt} = i_L - \frac{v_e - V_{EE}}{R_e}$$

$$C \frac{dv_c}{dt} = C \frac{dv_e}{dt} + i_L - i_c$$

where  $i_c$  is the forward transistor collector current defined by  $i_c = \gamma(e^{-\alpha v_e} - 1)$ ,  $\gamma$  and  $\alpha$  are empirically derived factors for the transistor and  $R_L$  is the series resistance of the inductor.

The second reason for choosing the Colpitts oscillator is apparent from both the circuit mathematical expression and the circuit schematic diagram. The Colpitts circuit is a simple circuit easily modeled, easily realized, and scaleable in frequency. These are critical factors in considering this type of architecture for practical, commercial technology.

The third reason is that in general the chaotic dynamics produced by this oscillator are well understood. There are parameter sets that produce chaotic oscillations of a Rössler type. Once such set of parameters are: [ $V_{cc} = 5V$ ,  $V_{ee} = -5V$ ,  $C = 1.6$  nF,  $C_e = 1.8$  nF,  $L = 6.8$   $\mu$ H,  $R = 62.5$   $\Omega$ ,  $R_L = 2\Omega$ ,  $R_e = 260\Omega$ ,  $\gamma = 1.06 \times 10^{-15}$ ,  $\beta = 41.2$ ]. Figure 2.3 shows the output oscillation for  $v_c$  with respect to time, and figure 2.4 shows a three dimensional plot of the solutions of the state equations for the circuit utilizing these parameter values. The object formed is what is termed a *state-space attractor*, and is

indeed a strange attractor. Figure 2.5 shows the power spectrum for  $v_c$ . Here we see the broad spectral content typical of chaotic oscillations. The calculated resonant frequency for the circuit, using the equation above, was 2.1 MHz.

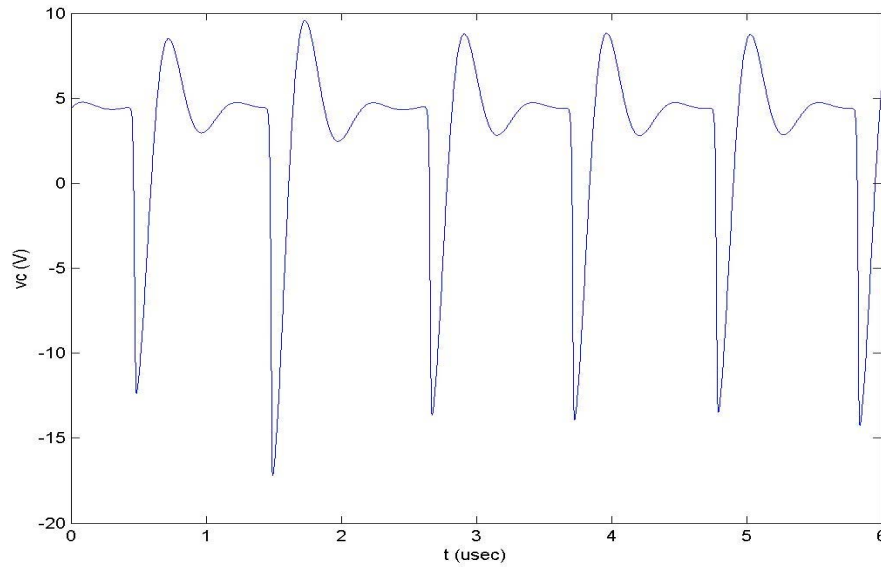


Figure 2.3 Collector voltage versus time for the Colpitts circuit using a parameter set that produces Rössler type chaos.

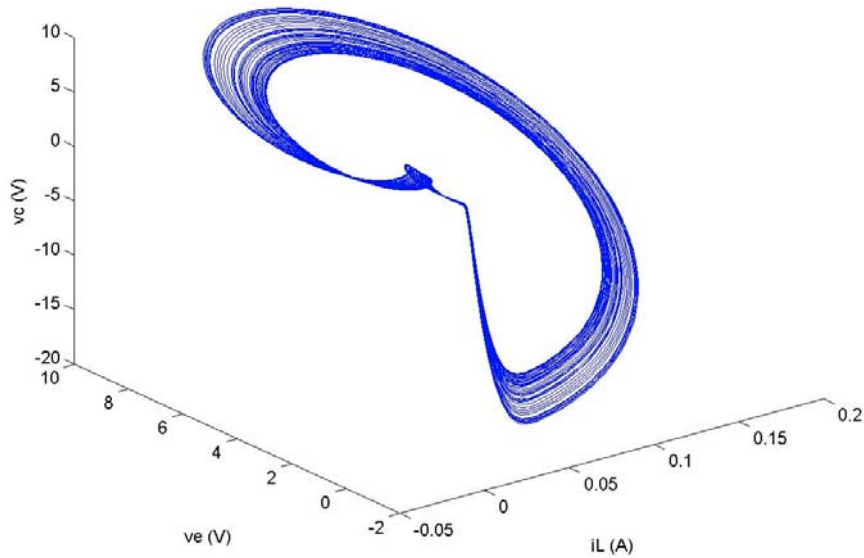


Figure 2.4 Three-dimensional representation of the state-space trajectories for the Colpitts oscillator illustrating the Rössler band.

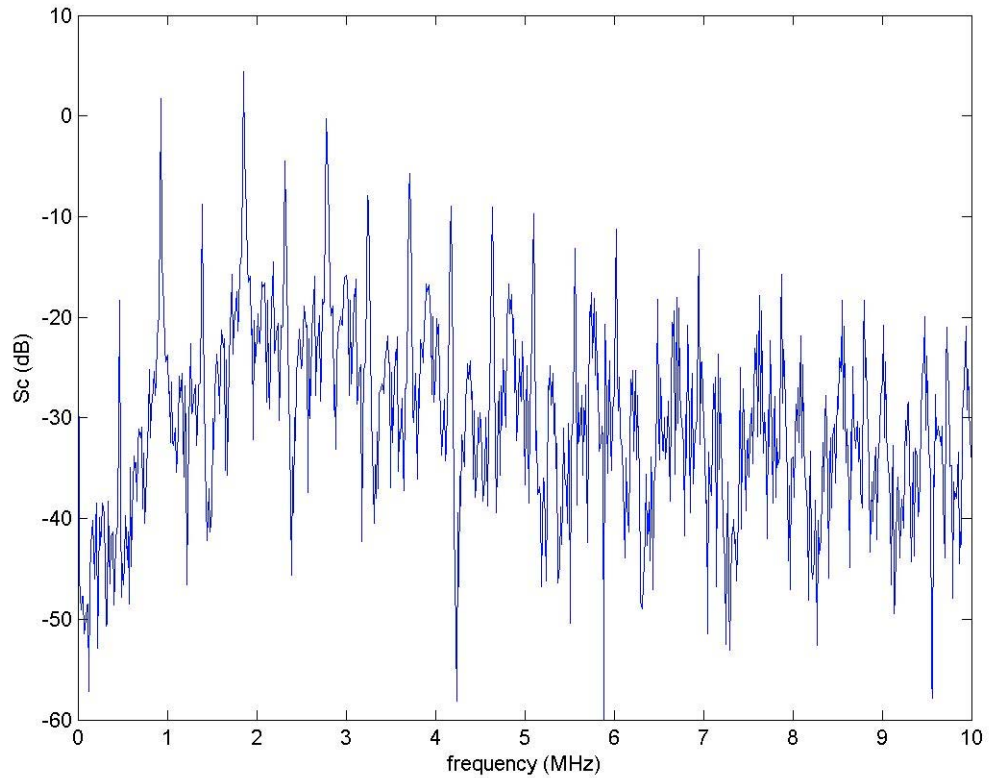


Figure 2.5 Power spectrum of the collector voltage for the Colpitts oscillator in a chaotic mode of operation.

Different parameter values yield different degrees of chaotic behavior. This will become useful for tuning and optimization of performance in specific applications. In the next section we will show how this continuous-time chaotic oscillation is related to a one-dimensional discrete-time map, and thus derive some of the measures developed earlier for the logistic map.

## 2.2 Properties and Measures

One of the most significant tools in the analysis of chaotic dynamics is the Poincaré surface of section [5]. Named for the early 20<sup>th</sup> century French mathematician Henri Poincaré, the Poincaré surface of section is a way of reducing a three-dimensional continuous-time flow to a discrete-time map by placing a two-dimensional surface in the path of the flow and extracting the points that pierce that surface. Figure 2.6 illustrates the placement of such a surface in the state-space for the attractor of figure 2.4. Figure 2.7 shows the resulting Poincaré map while figure 2.8 gives the *return map* for the collector voltage. Although these maps appear to be one-dimensional, and can be approximated as such, there is a highly compressed Cantor set fractal that governs the placement of each point of the mapping [13]. Note the similarities of the return map to the logistic map.

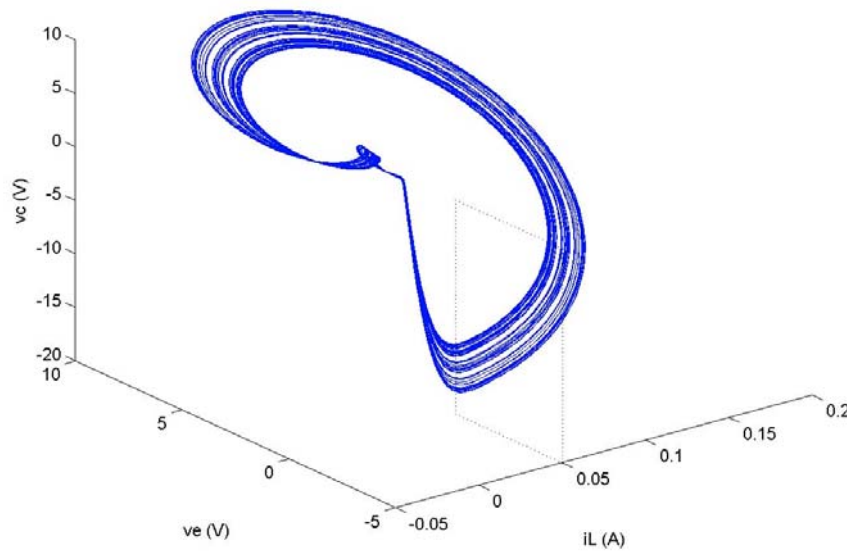


Figure 2.6 Chaotic attractor for the Colpitts oscillator with an Poincaré surface of section erected in the flow.

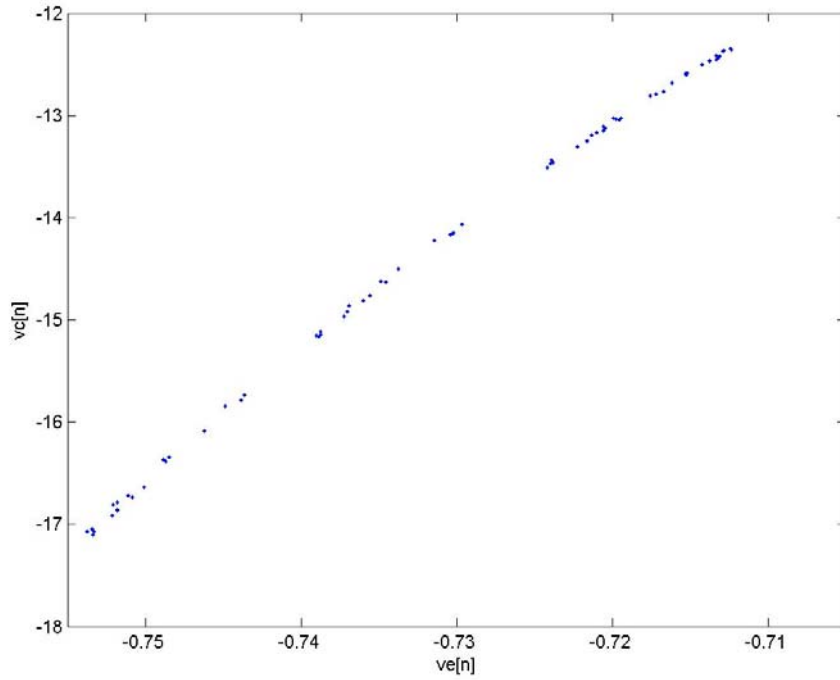


Figure 2.7 Poincaré map produced by the surface of section in figure 2.6.

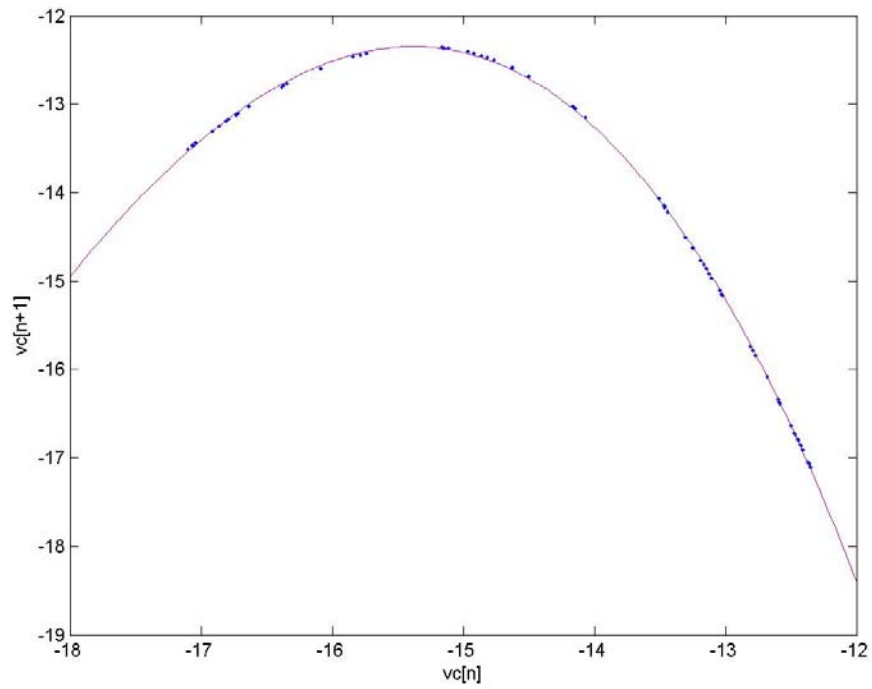


Figure 2.8 Return map for the collector voltage as produced by sequential observation of points generated by the Poincaré mapping. Note its resemblance to the logistic map.

Given the similarity to the logistic map we can calculate a Lyapunov exponent in a similar fashion. It is important to note that Lyapunov exponents are dependent upon the region of state-space from which the trajectories originate. Large, positive exponents indicate regions of tremendous expansion of the attractor while smaller exponents indicate a slower rate of expansion. Both actions are necessary for chaotic motion. Chaotic oscillations achieve a balance between instability and degeneration, thus we have termed these oscillations as *bounded instabilities*. Table 2.1 shows calculated Lyapunov exponents for two sets of points using the Colpitts oscillator discrete-time mapping. The results illustrate the compression and expansion of the flow.

Table 2.1 Calculation of local Lyapunov exponents for the discrete time mapping of the Colpitts oscillator.

$v_0$	$d_0$	$v_N$	$d_N$	$\lambda$
-14.1593	--	-17.0695	--	
-14.0679	0.0915	-14.0679	3.0016	0.5036
-12.427	---	-13.2497	---	
-12.4248	0.0022	-13.1887	0.0610	0.4793



### 2.3 The Colpitts Oscillator as a Digital Signal Source

If we take a further step and assign a partition boundary to the discrete-time return map for the chaotic flow, we can produce a unique symbolic representation of the dynamics of the system [21]. A natural partition boundary exists at the peak of the map. The partition also lends itself to the simplest symbolic representation, binary. Figure 2.9 shows the assignment of the symbolic dynamics to the return map and indicates how binary information is generated by the oscillations. Figure 2.10 shows how this partition is related to the Poincaré map, which is directly related to the chaotic flow.

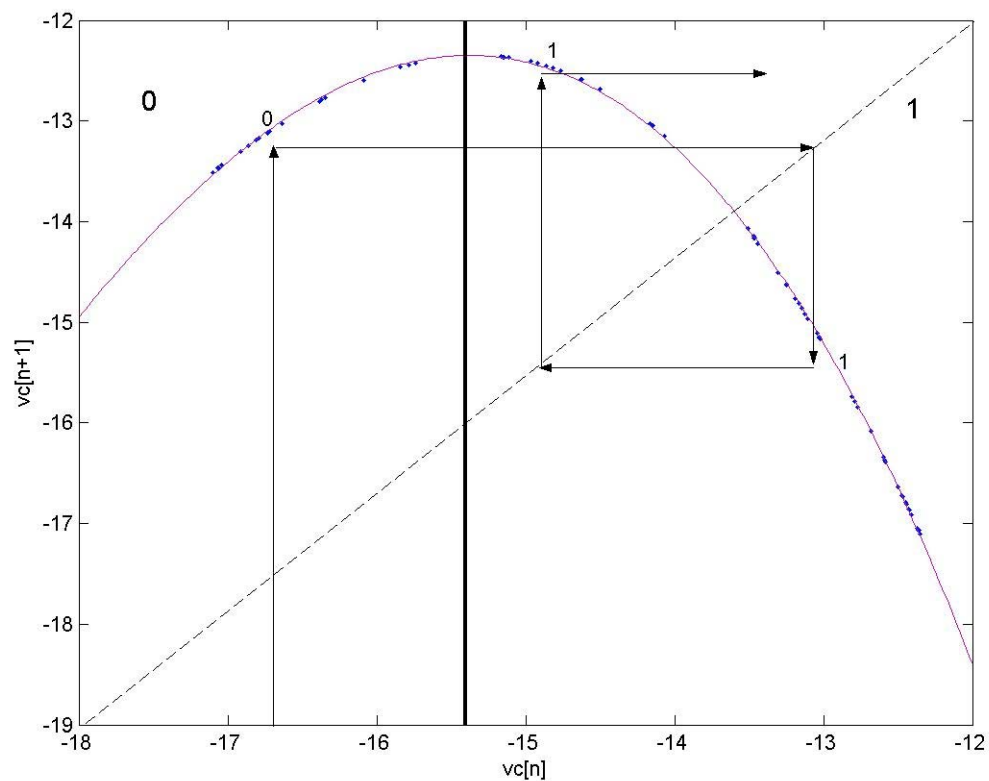


Figure 2.9 The return map for the Colpitts chaotic oscillator illustrating the binary partition and the generation of digital information.

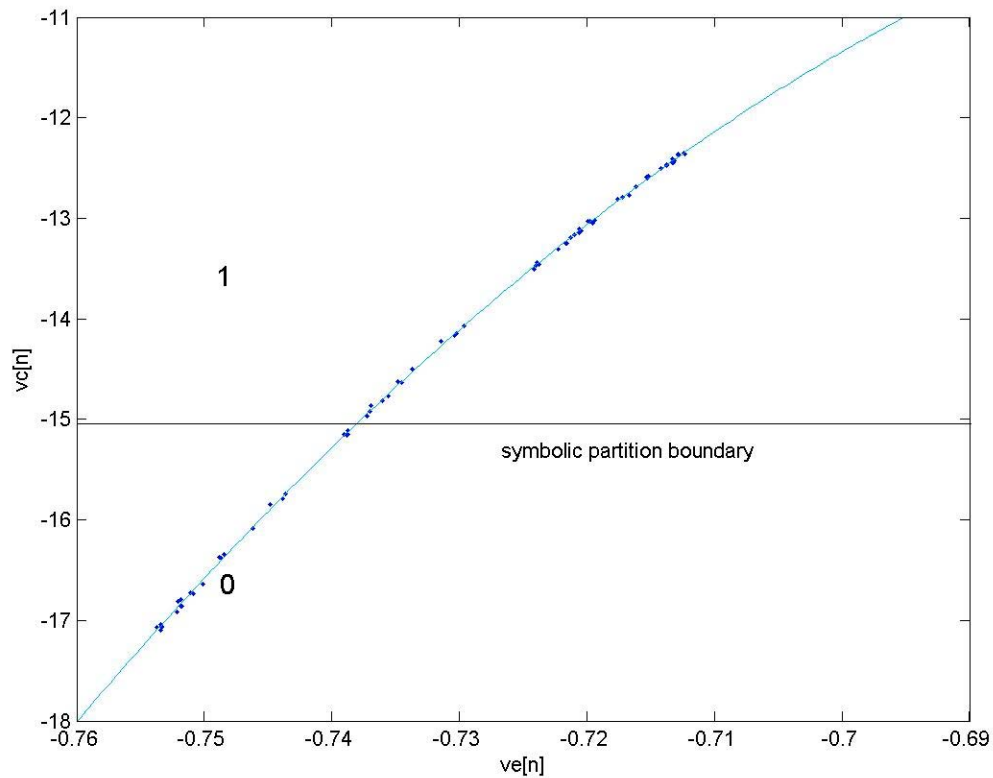


Figure 2.10 The Poincaré map of the Colpitts chaotic oscillation showing the placement of the binary partition boundary. Trajectories passing through the Poincaré surface of section on either side of the boundary produce bit 0 or 1.

We can take this analysis a step further by considering the  $N$ -bit binary sequences generated when a trajectory crosses a particular point on the Poincaré surface. This is done by integrating the system forward in time and capturing the bits in an  $N$ -bit register as state-space trajectories cross the surface. The result is the  $N$ -bit *coding function* that gives the proper state-point necessary for generating a given binary sequence. We show an example of this coding function for 8-bit binary sequences in figure 2.11. The 8-bit sequences are represented by their decimal numbers from 0 – 255 (00000000 – 11111111). The parameter set used to generate the chaotic oscillation produce highly constrained symbolic dynamics. This is evident from the attractor in figure 2.6. Note that

the band of chaotic trajectories is then and does not fill the state space from the center outward. As a result, only 20 of the possible 255 8-bit binary sequences are generated for the number of integration steps taken.

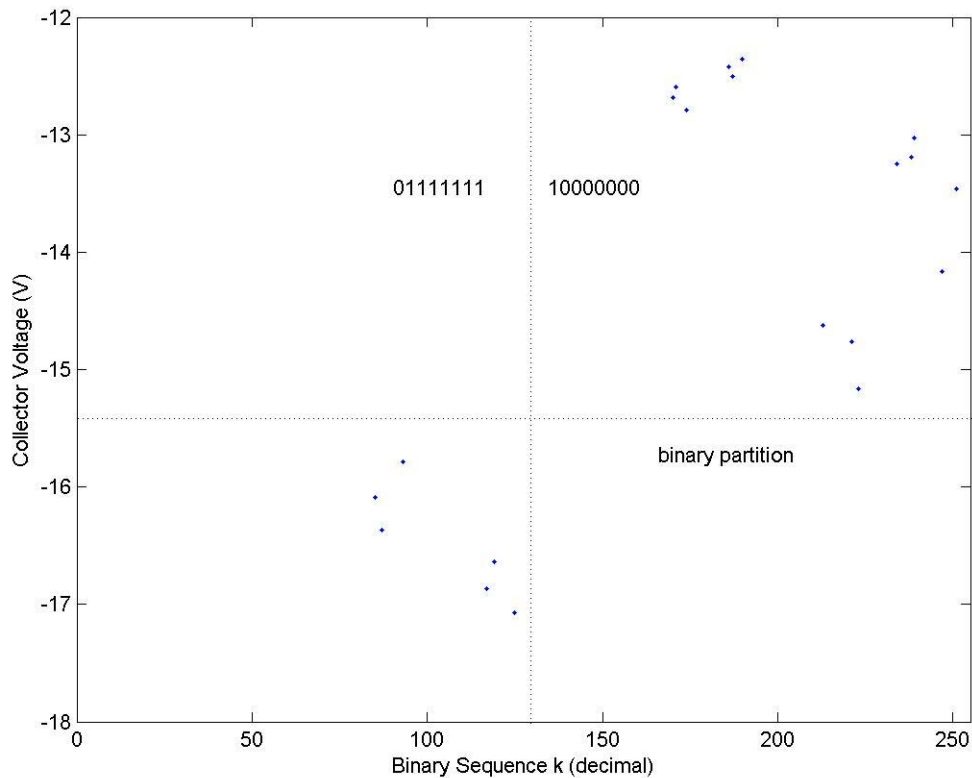


Figure 2.11 8-bit binary coding function for the Colpitts oscillator.

The Poincaré surface of section is placed at a point in the state space where  $i_L = 0.05$  A. Each binary sequence is uniquely associated with a collector voltage via the coding function and a emitter voltage via the Poincaré map. The conclusion is that there is a unique point in state space that will be a source for a distinct binary sequence. This point can be used as an initial condition to encode binary information into the chaotic oscillations. Hayes work involved using small perturbations to control a chaotic

oscillator to produce any desired digital stream [15]. We show an example by encoding the 8-bit binary sequence 01011101 (decimal 93).

According to our coding function and Poincaré map, the initial condition that will source this sequence in the chaotic oscillation is  $i_L = 0.05$ ,  $v_e = -0.7438$ , and  $v_c = -15.7858$ . Figure 2.12 shows this oscillation in state space while figure 2.13 shows the collector voltage with respect to time with the Poincaré surface crossings marked to show the binary encoding.

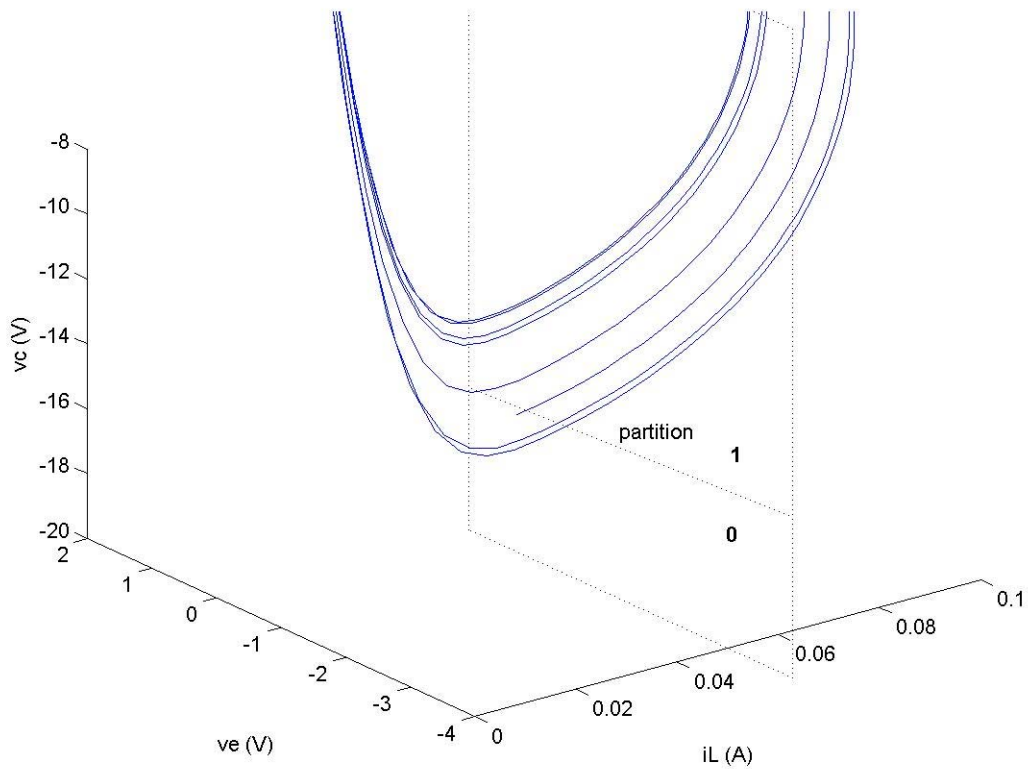


Figure 2.12 State-space trajectories encoded to produce the 8-bit binary sequence 01011101.

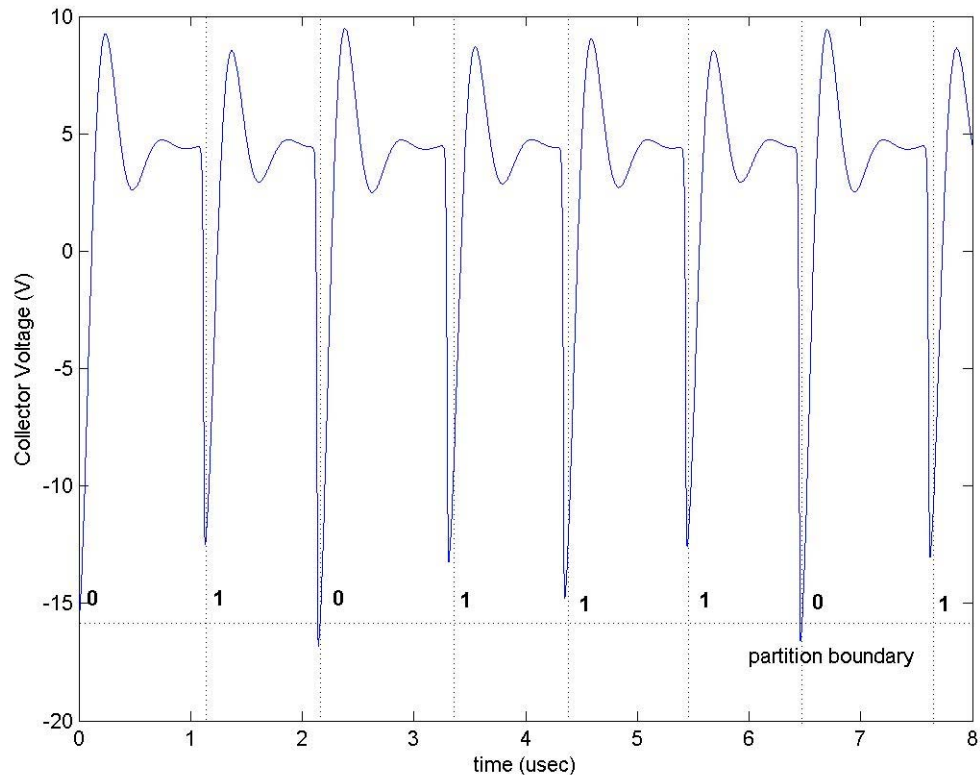


Figure 2.13 Time-varying collector voltage demonstrating the 8-bit binary encoding 01011101 embedded into the oscillations.

So far we have shown that a chaotic oscillator can be used as a binary signal source. Work has been done to provide further advances in the implementation of chaotic oscillators as digital signal generators. Innovations such as *segment hopping* [18] and band-limited, digitally encoded chaotic waveforms for base-band signaling [19] are being prepared for commercialization. The simplicity and efficiency of electronic chaotic oscillators are the primary attraction for technologists. In the next section we outline an implementation of chaotic dynamics to communication technology that provides tremendous advantage over traditional design.

## 2.4 Syncrodyne Amplification

The general concept of “controlling chaos” encompasses many different approaches. The first method to become widely accepted was the method of Ott, Grebogi, and Yorke, and became referred to as the OGY method of controlling chaos [10]. This method is essentially proportional feedback, and is used to control a chaotic oscillator so that it produces a periodic orbit. A control pulse is applied to a system with the pulse energy being proportional to the error from the desired periodic orbit. This method can also be used for symbolic dynamics control we referred to in the previous section. For symbolic control, the error is measured from the point in state space that sources the *desired* symbol sequence instead of a periodic point, and a proportional control pulse is applied to correct this error. One can also use continuous-time feedback control, and continuously correct the error from the desired trajectory in state space.

The problem with feedback methods for high frequency oscillators is their latency time. The controller must detect the error in state space, typically at the Poincaré surface of section, and then compute and apply a control pulse proportional to this error. This computation, be it digital or analog, takes time, and this loop delay can become a significant fraction of the Poincaré return time for rf oscillators. The synchronization property of chaotic systems provides an intriguing opportunity for engineering application.

The Syncrodyne amplifier based on the concept of signal amplification using **synchronous dynamics**. Syncrodyne amplification is the process of locking a chaotic oscillator, larger in power, to a smaller, continuous-time, information-bearing oscillator. The smaller oscillator is called the guide signal. The key is that the guide signal is

capable of carrying arbitrary digital information. Information transfer and power amplification is achieved.

The continuous-time guide signal has the advantage of only needing to guide one state variable. The guide signal need only supply a small amount of power to the "amplifying oscillator" in order to stabilize its dynamics. The result is that this type of continuous-time control of chaos acts as a signal amplifying means with great potential for digital communication applications. Figure 2.14 shows a simple block diagram of a syncrodyne amplifier. As synchronization occurs, the error signal,  $e(t)$  goes to zero. In a practical application, which we will describe shortly, this error is directly related to the current flow from the guide system to the output oscillator. As the current goes to zero the power flow from guide to output goes to zero and power amplification occurs.

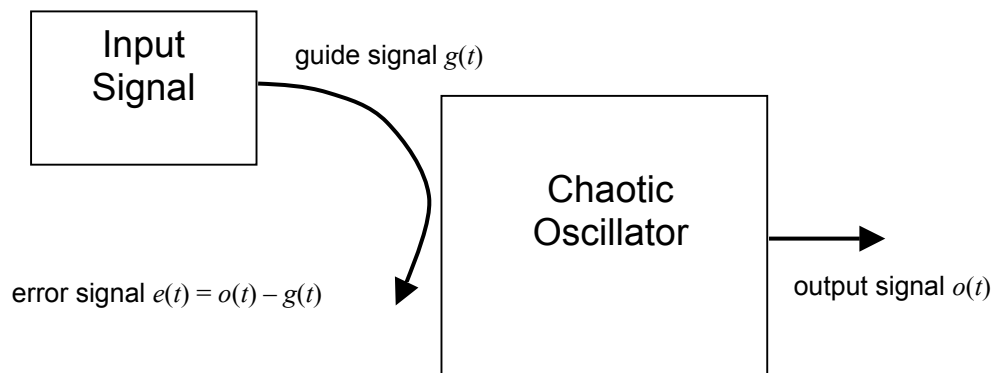


Figure 2.14 Block diagram of a Syncrodyne amplifier system.

It was once thought that this process would only apply to a guide oscillation and an output oscillation that has similar, if not exact, dynamical behavior. We show that this is indeed not the case. We show that the guide signal can be phase modulated sinusoidal oscillations such as phase shift keying (PSK), quadrature phase shift keying (QPSK), minimal shift keying (MSK) and even more sophisticated communications signal formats applicable to the global system for mobile communication (GSM) and code-division multiple access (CDMA). This leads to the application of this technique to standard digital communications technology, offering the possibility of high-gain, high efficiency power amplification.

We will use our Colpitts oscillator as our primary example. Consider the circuit shown in figure 2.15. It is the same as the earlier circuit although it is modified to accept an input signal at the emitter voltage node. The resistor  $R_{in}$  controls the input signal current. The circuit equations are modified as such,

$$L \frac{di_L}{dt} = V_{CC} - v_c - (R + R_L)i_L$$

$$C_e \frac{dv_e}{dt} = i_L - \frac{v_e - V_{EE}}{R_e} + \frac{v_{in} - v_e}{R_{in}}$$

$$C \frac{dv_c}{dt} = C \frac{dv_e}{dt} + i_L - i_c$$

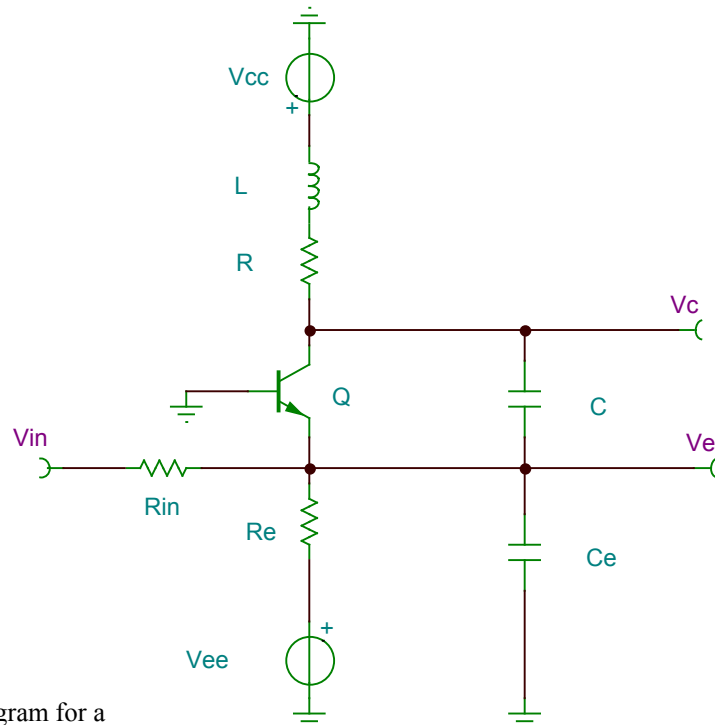


Figure 2.15 Circuit schematic diagram for a Colpitts oscillator based syncrodyne amplifier.



We will use this circuit to carry out our analysis via a MATLAB mathematical model. We will show results for sinusoidal input signals in the next section.

## 2.5 Modeling Results and Analysis

Before we show a series of results from our computer model we will first define some measures used in the analysis. First, we've chosen circuit parameters that put the resonant frequency near 2 MHz. Table 2.2 shows the values for the circuit used.

Table 2.2 Circuit parameter values used for syncrodyne amplifier model analysis.

Circuit Parameter	Value
$C$ (varied)	1 – 3 nF
$C_e$	1.8 nF
$R_e$	260 $\Omega$
$R_L$	2 $\Omega$
$R$	62.5 $\Omega$
$L$	6.8 $\mu$ H
$V_{cc}$	5 V
$V_{ee}$	-5V
$\gamma$	$1.06 \times 10^{-15}$
$\alpha$	41.2

Since we are analyzing the performance of a power amplifier the important measures are the power gain,  $G_p$ , and the *power added efficiency*, PAE. The gain is simply defined by  $G_p = 10\log(P_o/P_{in})$ , where  $P_o$  is the output power delivered to the load and  $P_{in}$  is the input power from the signal source. In this case we use  $R_e$  as the load. The

power added efficiency is an important measure in power amplifier analysis because it takes into account the power added by the source in its calculation. It is a much truer measure of the efficiency in such a case. In the model we calculate these power quantities by averaging over several cycles, thus obtaining these measures using average power. The following are the relationships between the power quantities and obtainable circuit values:

$$P_{dc} = P_{cc} + P_{ee}$$

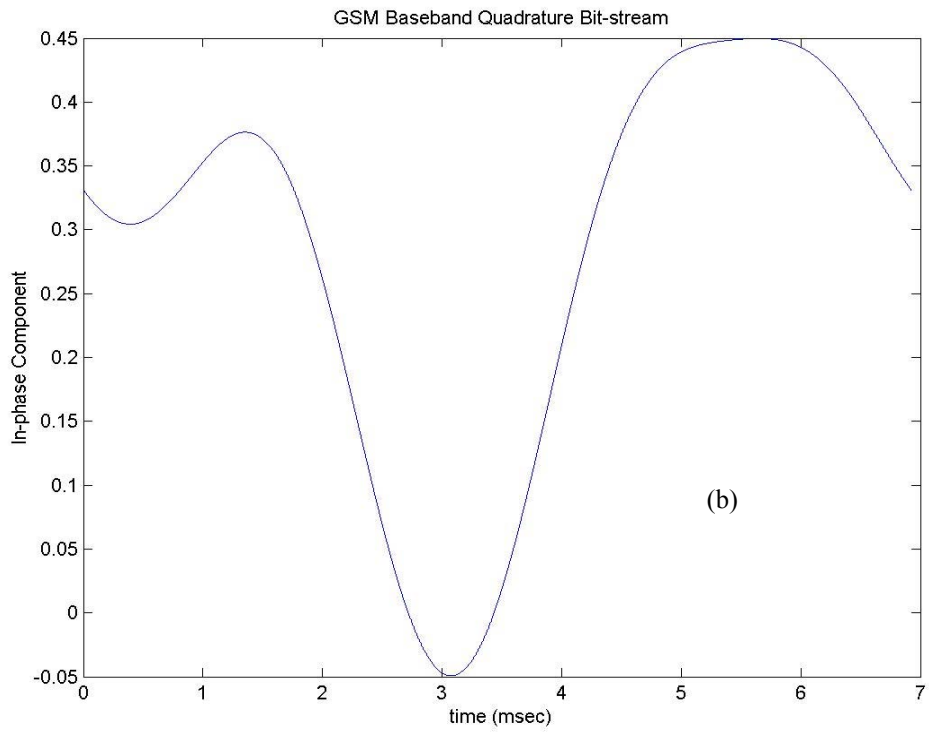
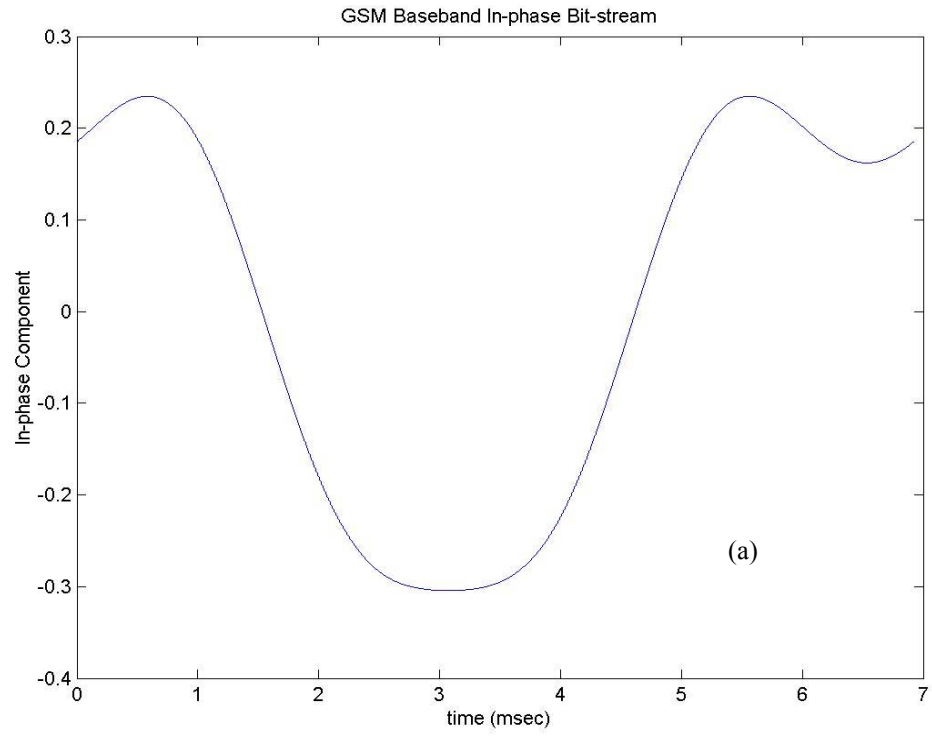
$$P_{cc} = V_{cc}i_L$$

$$P_{ee} = V_{ee}i_{Re} = \frac{V_{ee} - v_e}{R_e} V_{ee}$$

$$P_{in} = v_{in}i_{in} = \frac{v_{in} - v_e}{R_{in}} v_{in}$$

$$P_o = \left( \frac{V_{ee} - v_e}{R_e} \right)^2 R_e$$

The results to follow are generated using input signals that are produced using Gaussian-shaped minimal shift keying (GMSK) modulation technique. This modulation is used in the Global System for Mobile Communication (GSM) signal standard prevalent in wireless digital communications [20]. For typical GSM the carrier frequency will be 850 MHz and the digital information rate will be 270.833 Kbps. In order to have a comparable modulation scheme we generate a GMSK waveform with a carrier frequency of 2 MHz and a bit rate of 650 Hz. Figure 2.16 shows (a) the in-phase and (b) quadrature baseband waveforms (c) a section of the modulated carrier and (d) the power spectrum of the output waveform. Random binary information is used as the information stream. These are the waveforms amplified by our syncrodyne amplifier model.



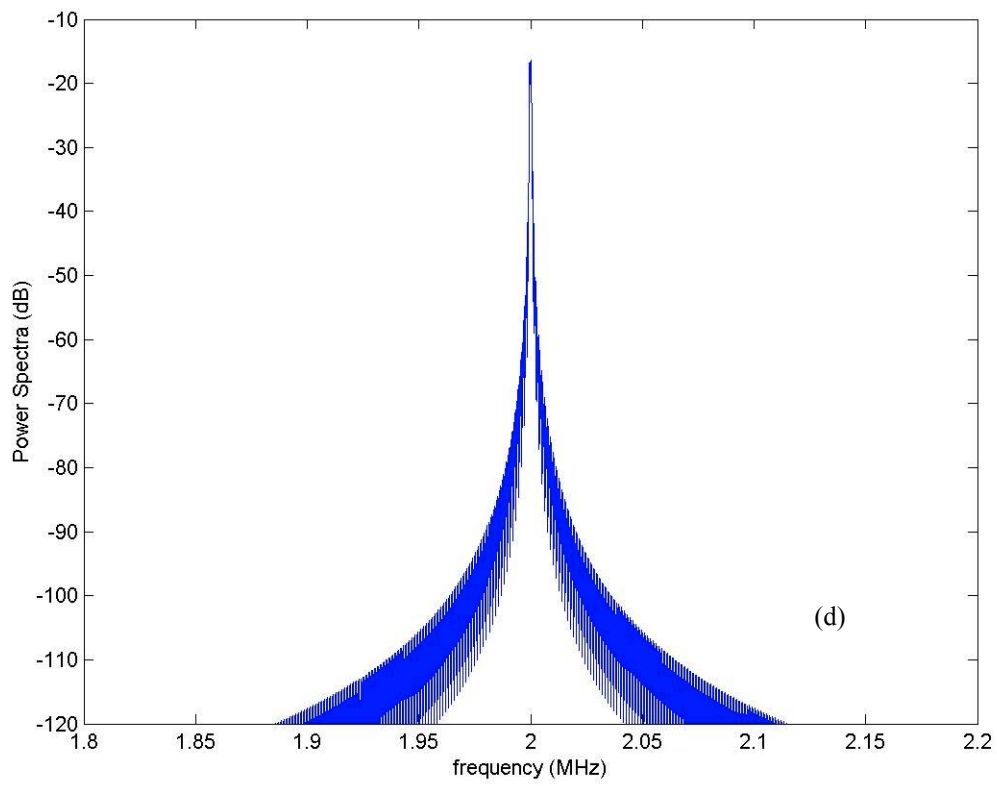
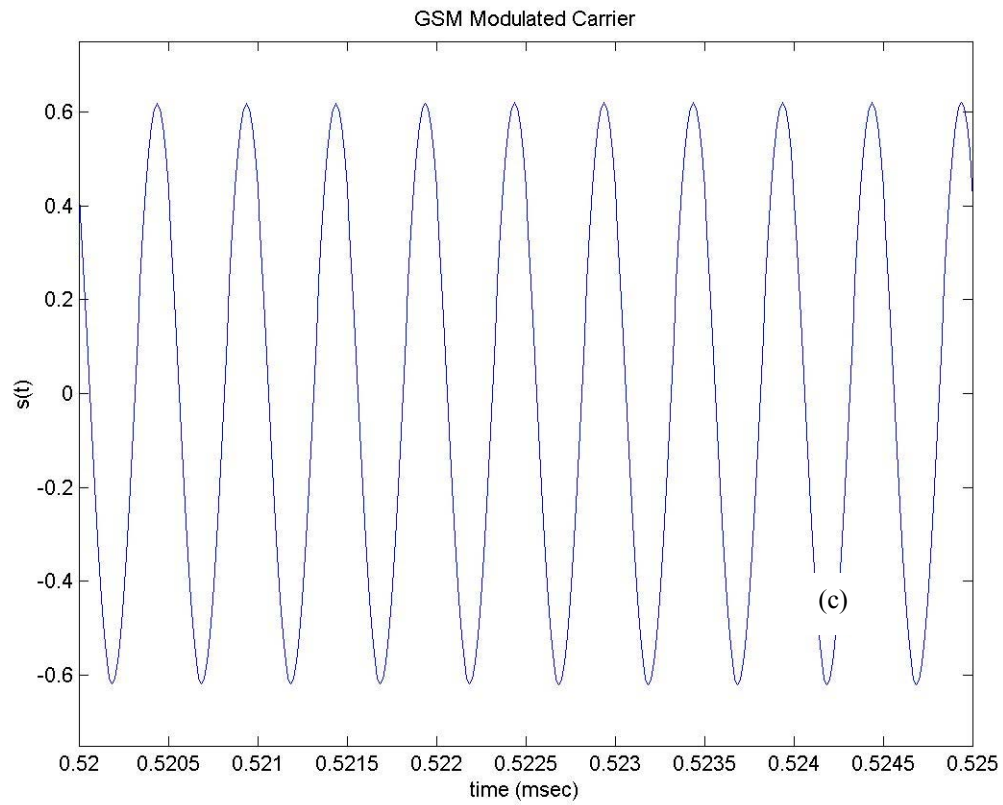


Figure 2.16 (a) In-phase and (b) quadrature baseband components of a 2 MHz GSM waveform along with (c) the modulated carrier and (d) the power spectrum.

A significant finding was that the capacitor  $C$  acted as an optimization element for the gain and the efficiency. We were able to maintain stable, repeatable chaotic dynamic in the circuit over a range of 1 nF to 3 nF. First we saw that the size of the attractor change as this element was varied. If we create a fictitious measure called the *attractor volume*, derived by calculating the volume of a cube created from the maximum and minimum values from the inductor current, emitter voltage and collector voltage, we can see the relationship of the chaotic attractor to this capacitance. Figure 2.17 shows the relationship over a range of capacitance.

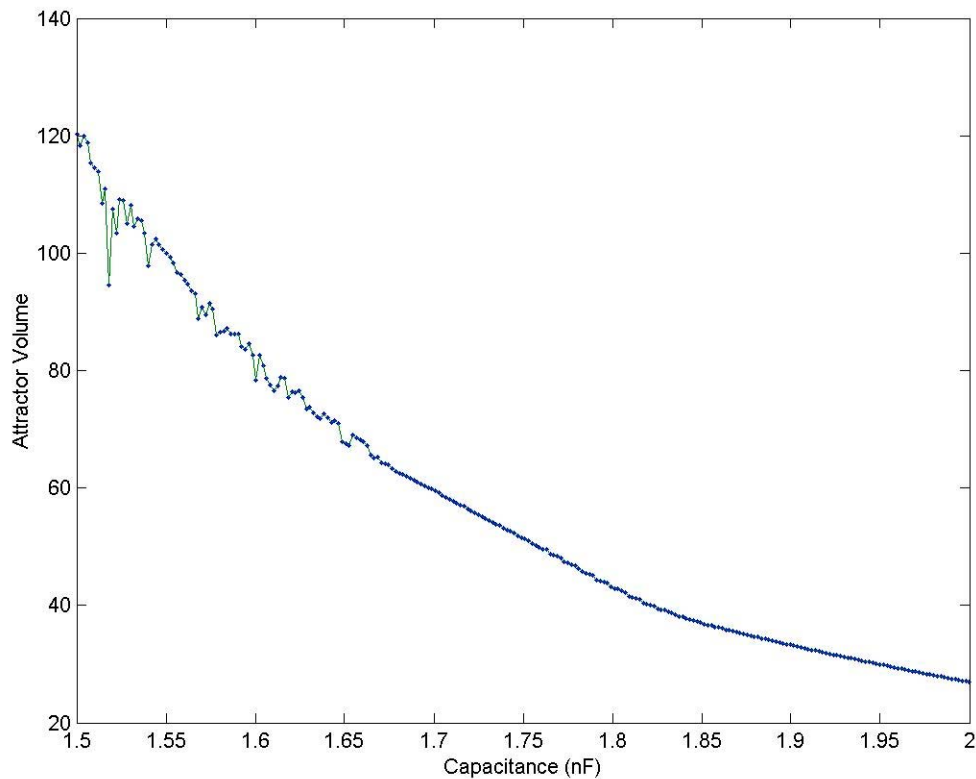


Figure 2.17 Variation of the attractor volume as the capacitor  $C$  is changed.

In the wireless handset power amplifier industry, the key challenge is the power-added efficiency. Typical power gain performance is about 30-dB. There are other industries,

such as satellite and base-stations, that may benefit from enormous power gains. The output signal power was maximum at about 25 dBm. We found that this tuning capacitor also allowed us to find points of enormous power gain. We surmise that these are points where the energy required to bring the chaotic oscillator in compliance with the source signal is nearly nonexistent. Figure 2.18 shows an example of power gains in excess of 60 dB for a given capacitor value. At this point we are not prepared to state that this relationship between the capacitance and the gain has a fractal structure to it, although it is possible. From a practical standpoint, we used an optimization algorithm to find the best capacitor value and similar procedures could be implemented with tuning capacitors such as varactors.

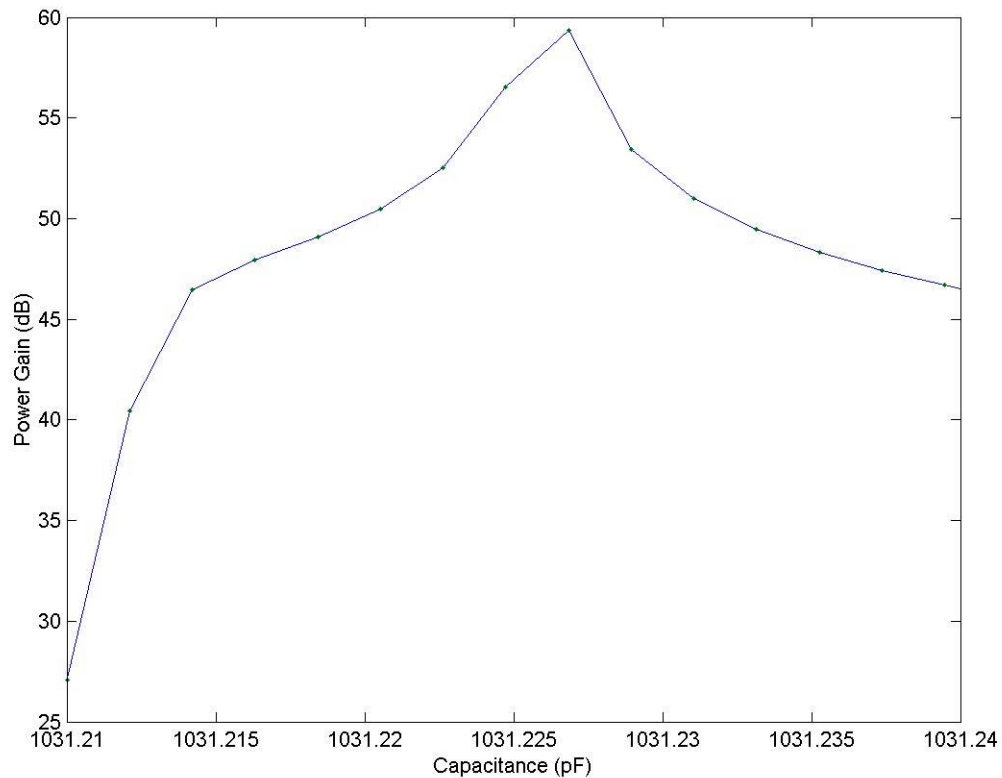


Figure 2.18 Power gain as a function of the tuning capacitance  $C$ .

As expected the efficiency of the amplifier was directly related to the peak-to-peak voltage of the input signal. The tuning capacitance also affected the efficiency. We were able to calculate a relationship between the peak-to-peak input voltage, the tuning capacitance and the power-added efficiency. This will allow a designer to determine the optimal range of operation for the amplifier. Figure 2.19 is a surface map that illustrates this graphically. Note that there is a wide range of operation for a designer to achieve 70% PAE or better from this system.

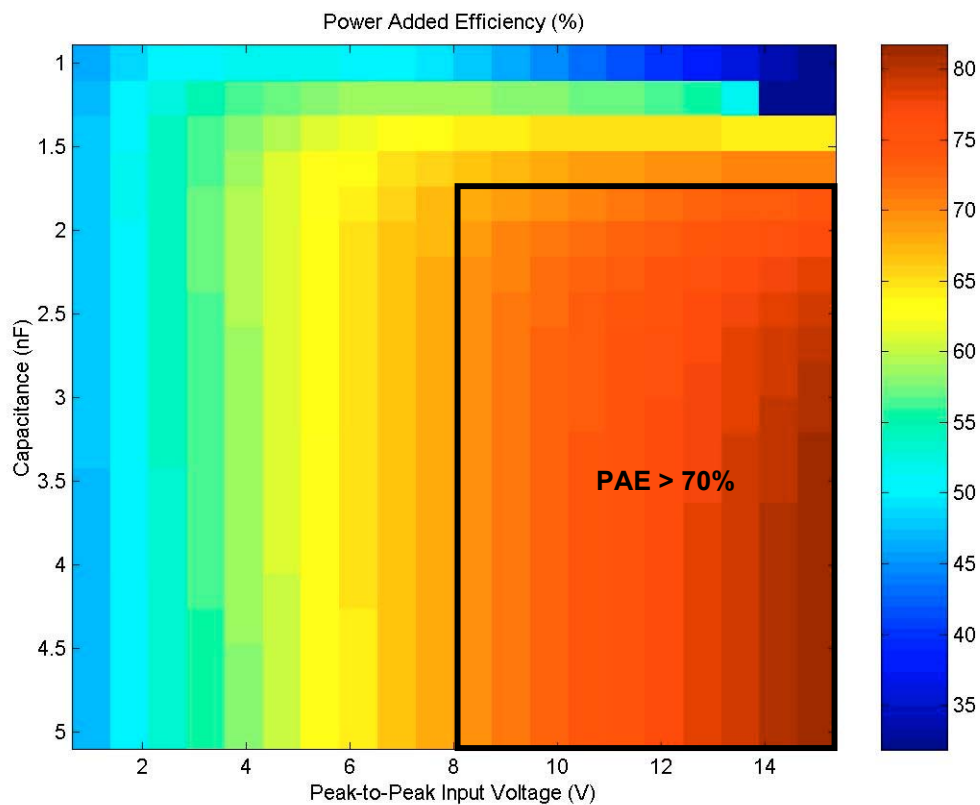


Figure 2.19 Surface map illustrating the PAE for peak-to-peak input voltages and tuning capacitance values.

In a similar manner we were able to calculate curves for the maximum power gain as the peak sinusoidal input voltage was varied. This acts as a complementary design tool. Figure 2.20 is a plot of this relationship. Higher power gains are probably possible as we tune the asymptotic relationship between the tuning capacitance and gain. We wanted, however, to stay within the bounds of realizable capacitor values. Finally we were able to determine the relationship between the optimal power gain and the optimal PAE for this system. This relationship is shown in figure 2.21.

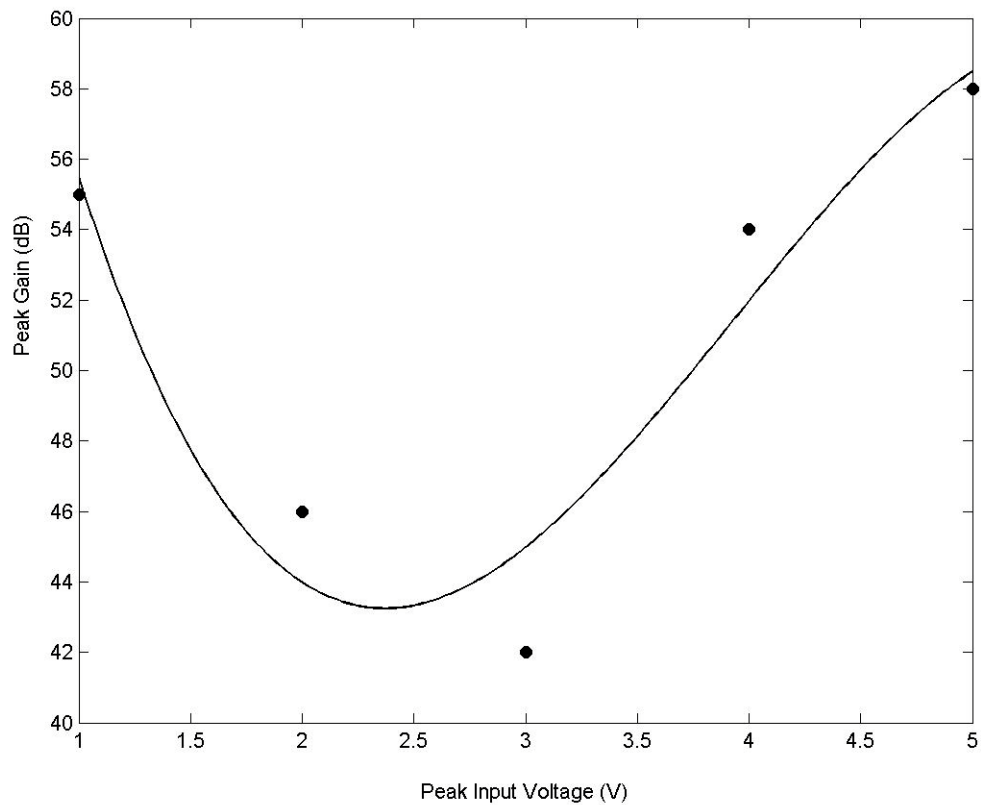


Figure 2.20 Relationship between the peak power gain and the peak sinusoidal input voltage for the syncrodyne amplifier circuit.



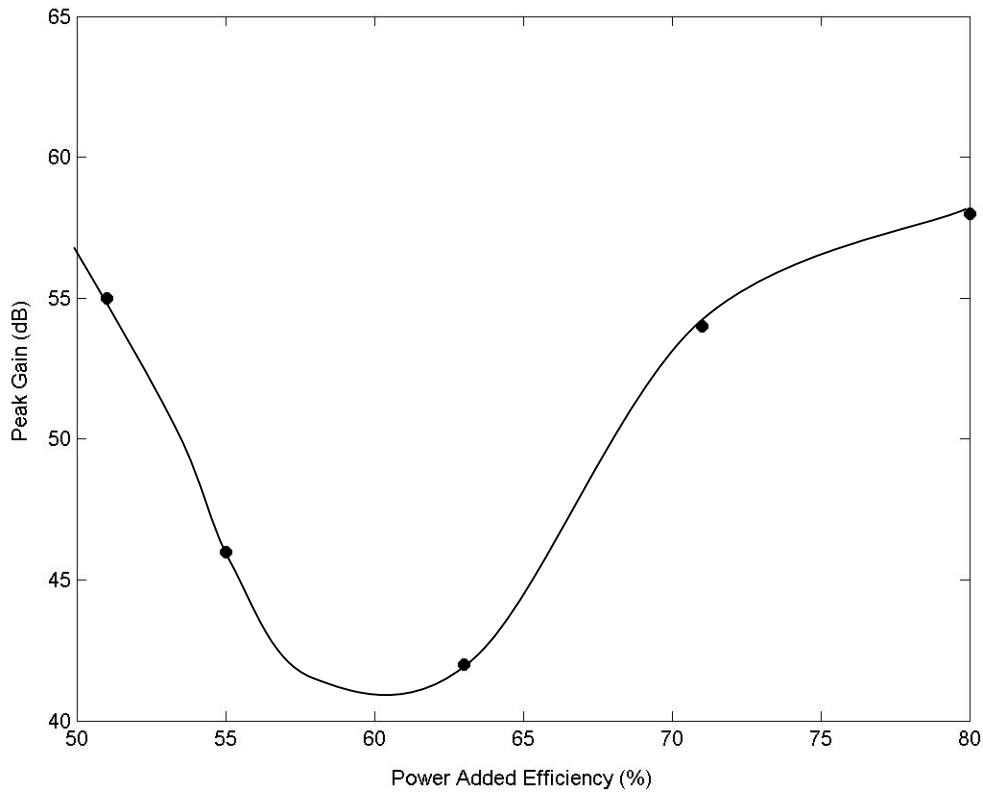


Figure 2.21 Overall PAE peak power gain relationship for the syncrodyne amplifier circuit. Note that there are regions of operation where the system is capable of nearly 80% PAE and greater than 55 dB gain.

In traditional power amplifier systems you would expect to find a linear, inverse relationship between gain and efficiency. In this system the relationship is not simple. It suggests that high gain and high efficiency are possible in various regions of operation. The tradeoff appears to be in the system stability. It is difficult to maintain the areas of extremely high gain in practice. System noise and component tolerances will make the tuning of extremely high-gain points impractical. Practical gain numbers should be about 40-dB.

The goal of this work was to define and analyze a chaotic circuit capable of acting as a digital signal source. Not only have we modeled such a system that acts as a direct digital encoder by producing a binary symbolic dynamics, we have further modeled a

system capable of providing ultra-high power amplification and high power-added efficiency to standard communications waveforms such as GSM. We take this work a step further by carrying out the design, fabrication, and testing of the 2 MHz syncrodyne amplifier described in this chapter, and provide a formal approach for the design of a 850 MHz chaotic oscillator for implementation of the syncrodyne approach at PCS (personal communications systems) frequencies. This is outlined in the next chapter.

## CHAPTER 3

### Custom RF Chaotic Oscillator Design

#### 3.1 Design Criteria

In this chapter will the outline the fabrication and testing of a 2 MHz syncrodyne amplifier circuit and also show preliminary modeling results for an 850 MHz circuit. We began by looking at the modified circuit schematic diagram used in a PSPICE analysis, and use this for the basis for the PCB layout. Figure 3.1 shows a schematic diagram of this circuit.

One of the critical features of this circuit will be its ability to be tuned to different types of behavior. As we outlined in the first chapter, there are different types of dynamics that can be present in one chaotic system. We will need to be able to tune the circuit so that it produces the type of chaotic behavior we want to work with and also be able to tune the chaos to some of the different states possible within it. The variable resistors  $R_e$  and  $R_1$  are good for tuning the circuit from periodic behavior to the desired chaotic states. Once there,  $C_T$  is a variable capacitor used to maximize the gain and efficiency. Resistor  $R_{in}$  is used to adjust the synchronization of the input signal in order to maximize the performance. The figure also shows the element values used to realize this circuit.

The type of chaotic behavior desired is the *simply folded band*, which is a general description of a Rössler band, typical of a Colpitts oscillator in a chaotic state. Many other circuits produce Rössler-type behavior [21]. We have already shown how this type of chaotic motion is related to the single-humped, one-dimensional logistic map through the Poincaré surface of section. The analysis of these types of systems are more

manageable than more complex types of chaotic motion.

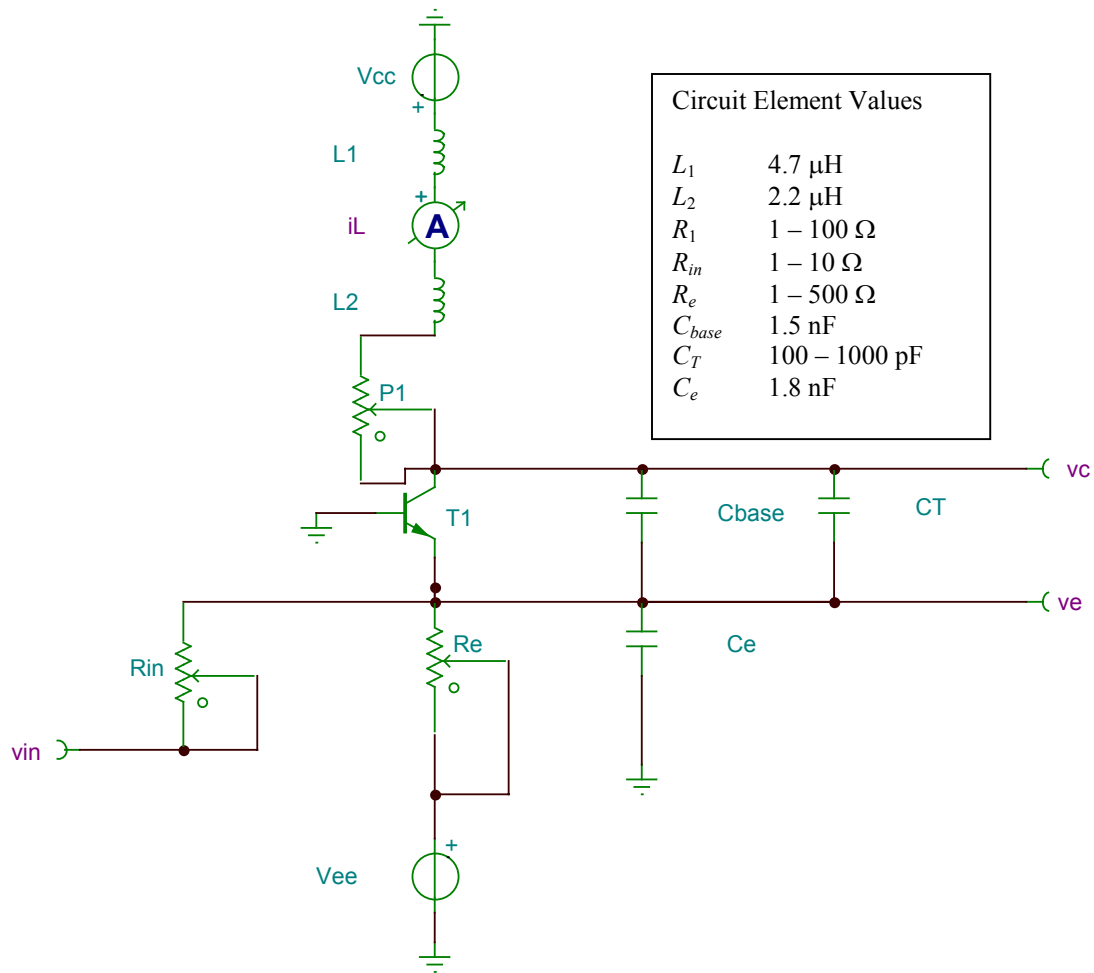


Figure 3.1 2 MHz syncrodyne amplifier circuit schematic diagram.

### 3.2 PSPICE Modeling

We were successful in generating a SPICE model for a 2 MHz chaotic oscillator capable of acting as a digital signal source via the control of symbolic dynamics and the application of syncrodyne amplification. The circuit schematic diagram of figure 3.1 was captured directly from the SPICE modeling package TINA. The following figures show the results from the model. The circuit is only slightly chaotic. The extreme limitations of the software to tune the circuit presented problems in generating various states of chaotic motion. As we will see in the following section, the actual fabricated circuit was more amenable to tuning.

Figure 3.2 shows a two dimensional projection of the state-space attractor, showing the inductor current versus the emitter voltage, which acts as our output. There is a small band of chaotic trajectories as the circuit settles into its steady-state from the initial off state. Note the slight fold that occurs in the trajectories. This action is necessary for simple chaotic motion. It was very easy to get this system to oscillate, however it was difficult to find broad chaotic motion. Figure 3.3 shows how the emitter voltage signal varies with respect to time. Note the irregular occurrence of the peaks. Figure 3.4 is the frequency spectrum of the emitter voltage signal. This demonstrates the broad frequency content typical of chaotic oscillations. The other important point is that this circuit architecture provides a method of producing chaotic motion that restricted to a limited frequency band. The property is attractive for communications applications, particularly wireless communications.

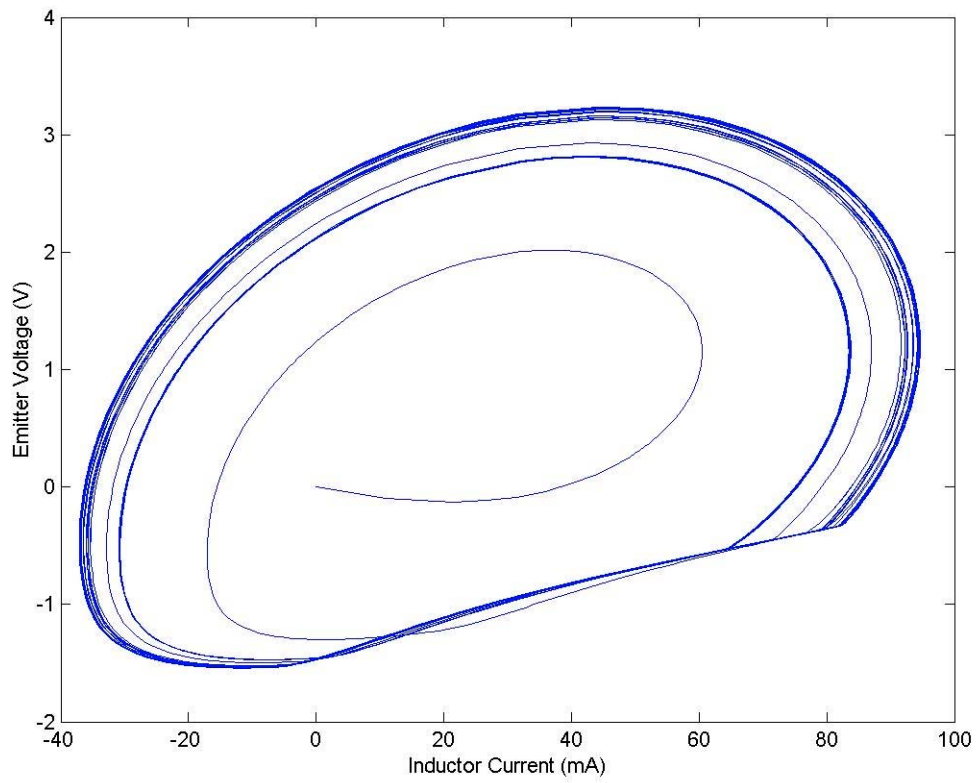


Figure 3.2 Two-dimensional projection of the chaotic attractor produced by the 2 MHz Colpitts oscillator SPICE simulation.

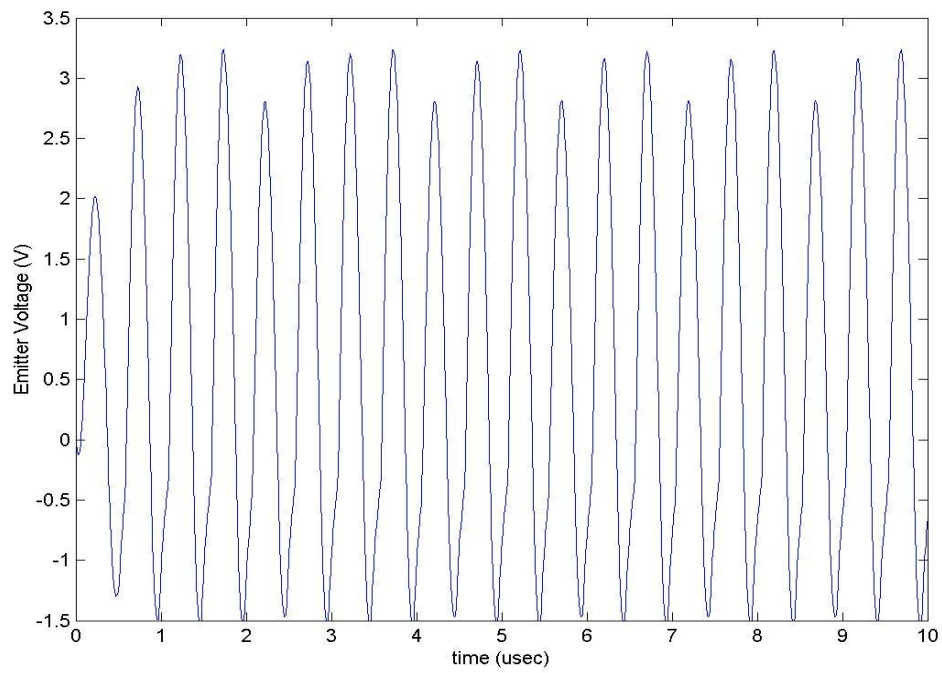


Figure 3.3 Time-dependent oscillation of the emitter voltage in a slightly chaotic state.

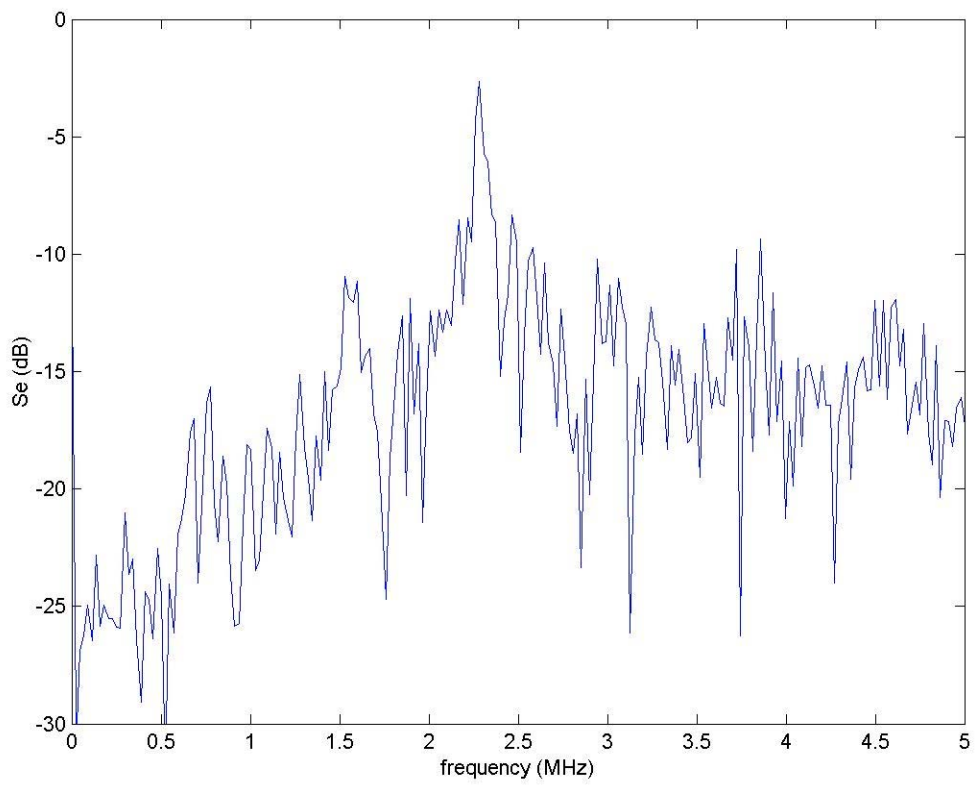


Figure 3.4 Frequency spectrum of the emitter voltage oscillations illustrating the broad frequency content indicative of chaotic behavior.

### 3.3 Circuit Fabrication and Testing

Figure 3.5 is a photograph of the fabricated 2 MHz Colpitts based chaotic circuit. The PCB layout illustrated in figure 3.6 was populated with circuit elements to realize the syncrodyne amplifier modeled in the last section. Some general measurements were taken. There was good agreement between the behavior of the mathematical model, the PSPICE model, and the fabricated circuit.

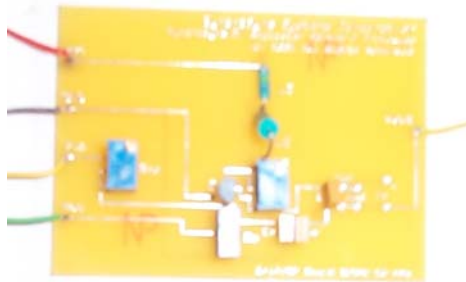


Figure 3.5 Photograph of the fabricated 2 MHz syncrodyne amplifier circuit.

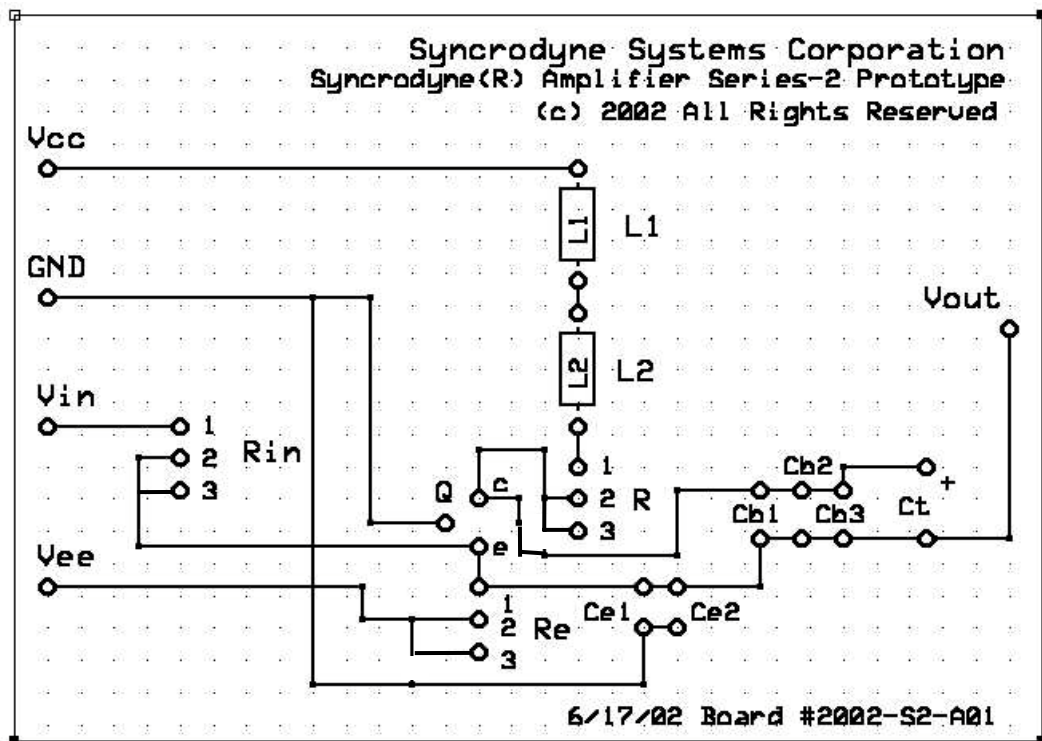


Figure 3.6 Picture of the PCB used to fabricate the 2 MHz syncrodyne amplifier circuit.



Figure 3.7 shows a measured time-dependent output signal from the circuit. Like the simulation, the chaotic motion is indicated by the irregular occurrence of the peaks and valleys. This, and the following measurements, were taken using a 40 Msps National Instruments sampling card. We had only one sampling channel available at the time of this measurement, allowing only one state-variable to be sampled at a time.

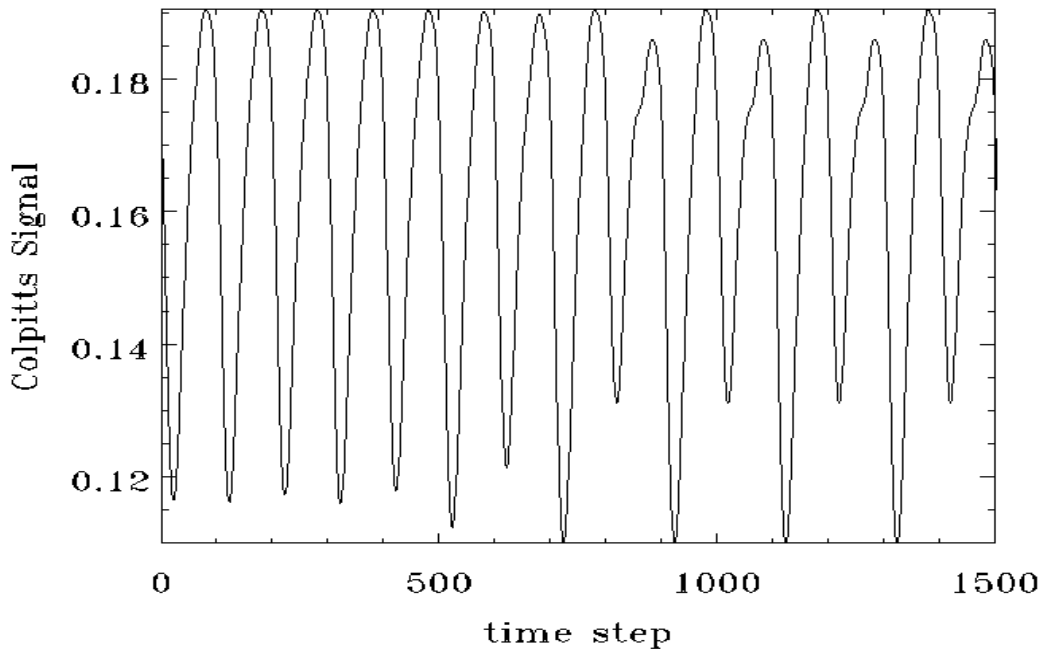


Figure 3.7 Measured time signal from the Colpitt's oscillator circuit.

Figure 3.8 shows the output data of the chaotic oscillator under symbolic dynamics control producing a constrained binary signal. First, the two-dimensional projection of the attractor is formed not by plotting two state-variables against themselves, but by

plotting one state variable versus a time-delayed copy of itself. This method is called *time delay embedding* and is useful when only one state variable of a chaotic system is available [22]. It is still possible to obtain a fairly accurate representation of the dynamics by using this method. The constraint on symbolic dynamics was introduced by disallowing any binary sequence that contained more than two consecutive zeroes. For example the sequence  $B_1 = 11100101$  would be allowed as an input, but the sequence  $B_2 = 11100010$  would not. There specific, identifiable regions of state-space that would produce sequenced with more than two zeroes present. These regions would never be visited by the trajectories, thus the gaps in the attractor.

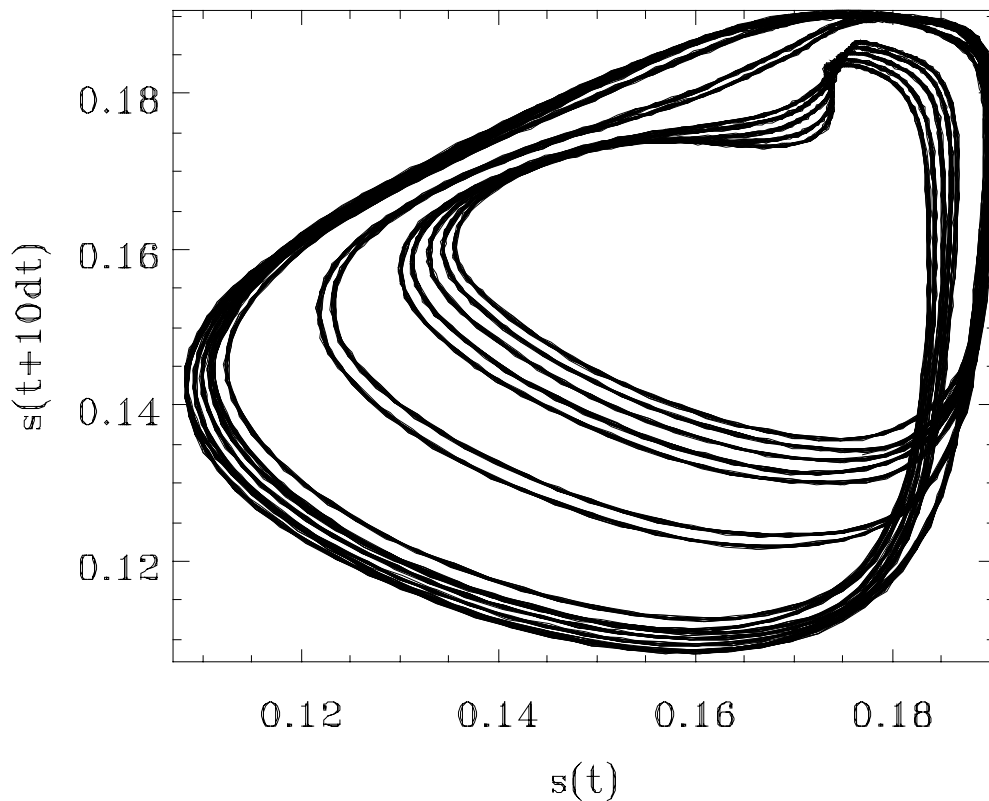


Fig. 3.8 The Colpitts attractor controlled on a constrained set. The Cantor set structure is a result of the constraint.

As we progressed in the testing phase of this project we were able to obtain a sampling card with two input channels. We were then able to measure two state variable simultaneously. Figure 3.9 shows a two-dimensional projection of the attractor using the voltage across the inductor,  $v_L$ , and the voltage across the collector capacitor. The inductor voltage is directly related to the inductor current  $i_L$ , which was used for earlier analysis. This attractor is produced using the chaotic circuit uninfluenced by any control signal. Figure 3.10 shows the same circuit controlled on a Cantor set using a constrained input binary sequence.

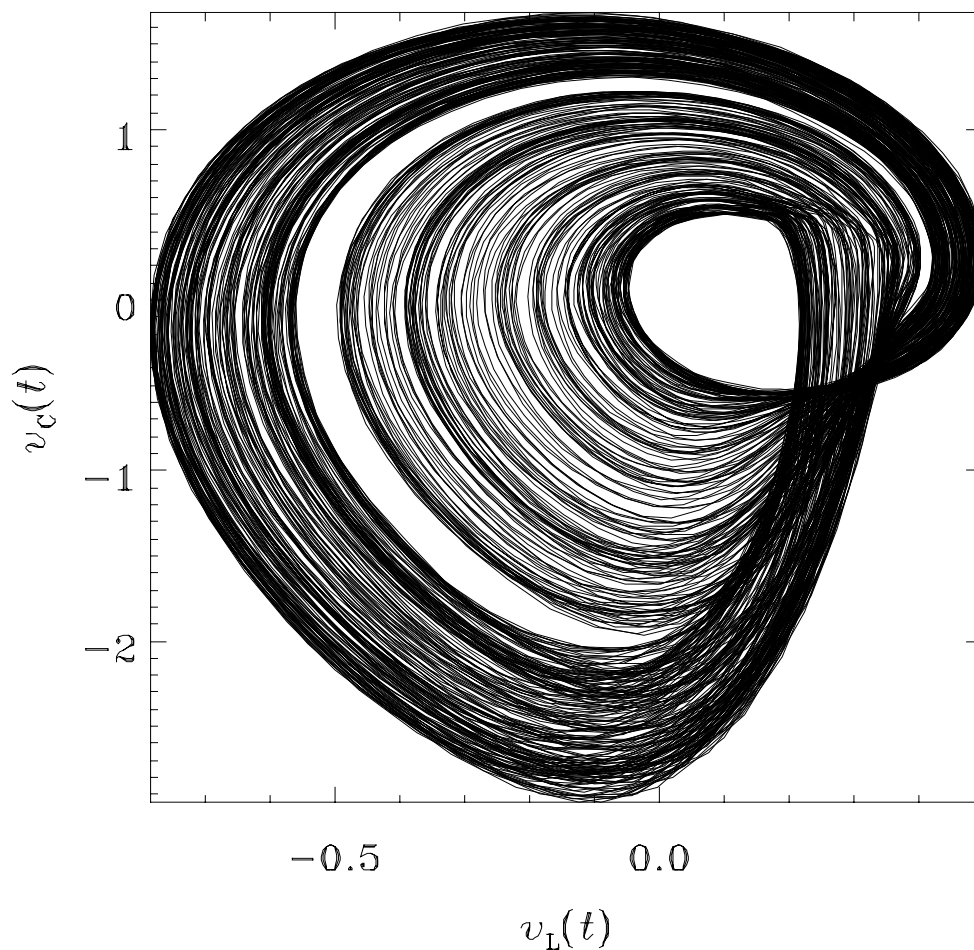


Fig. 3.9 Uncontrolled 2 MHz Colpitts attractor showing a two-dimensional projection of the state-space attractor.

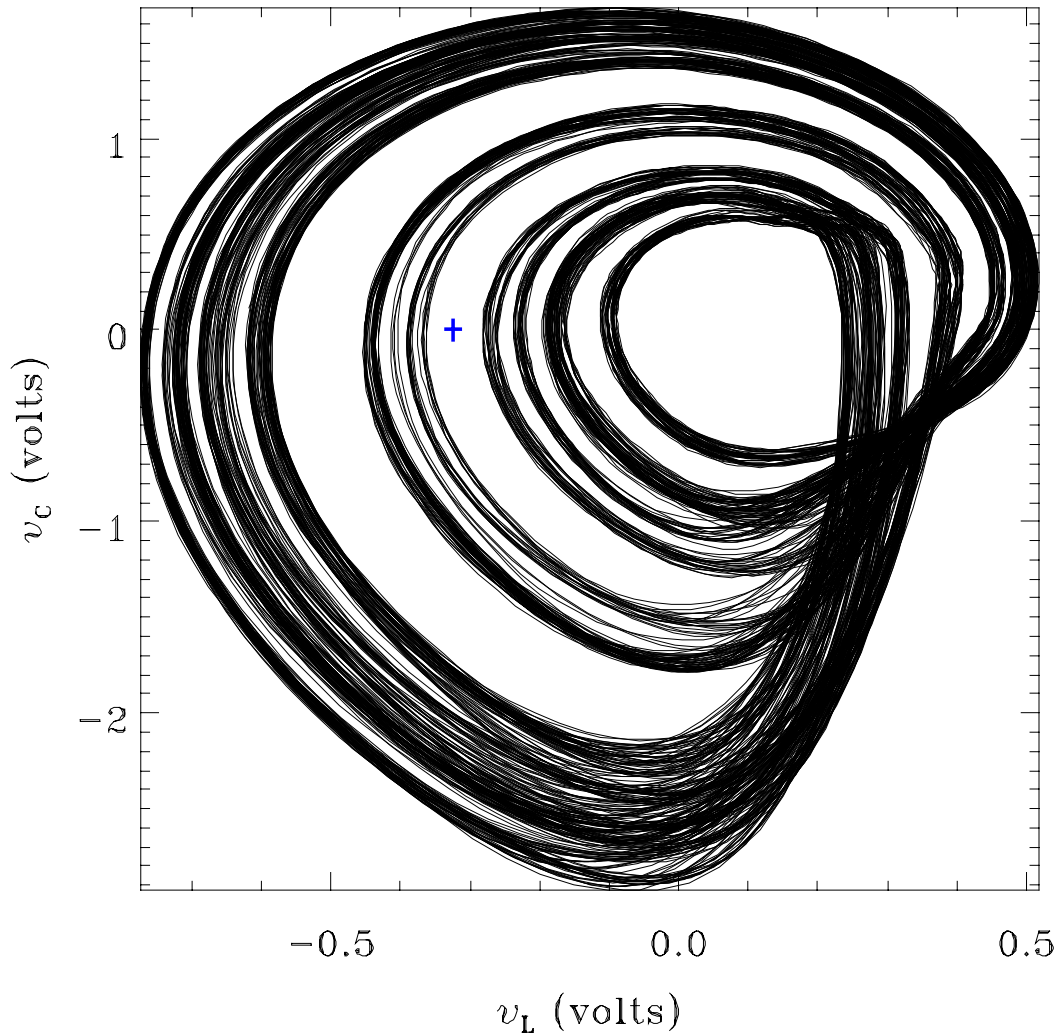


Fig. 3.10 Symbolic dynamics controlled Colpitts attractor.

Finally, we took measurements to demonstrate the syncrodyne amplification properties of the system. Figure 3.11 shows (a) the input signal, (b) the output signal and (c) the error signal. Although voltages are the same, the input power delivered as compared to the output power is extremely small, hence the enormous gain. Figure 3.12 shows comparisons of the measured experimental data with the modeled the data calculated earlier.

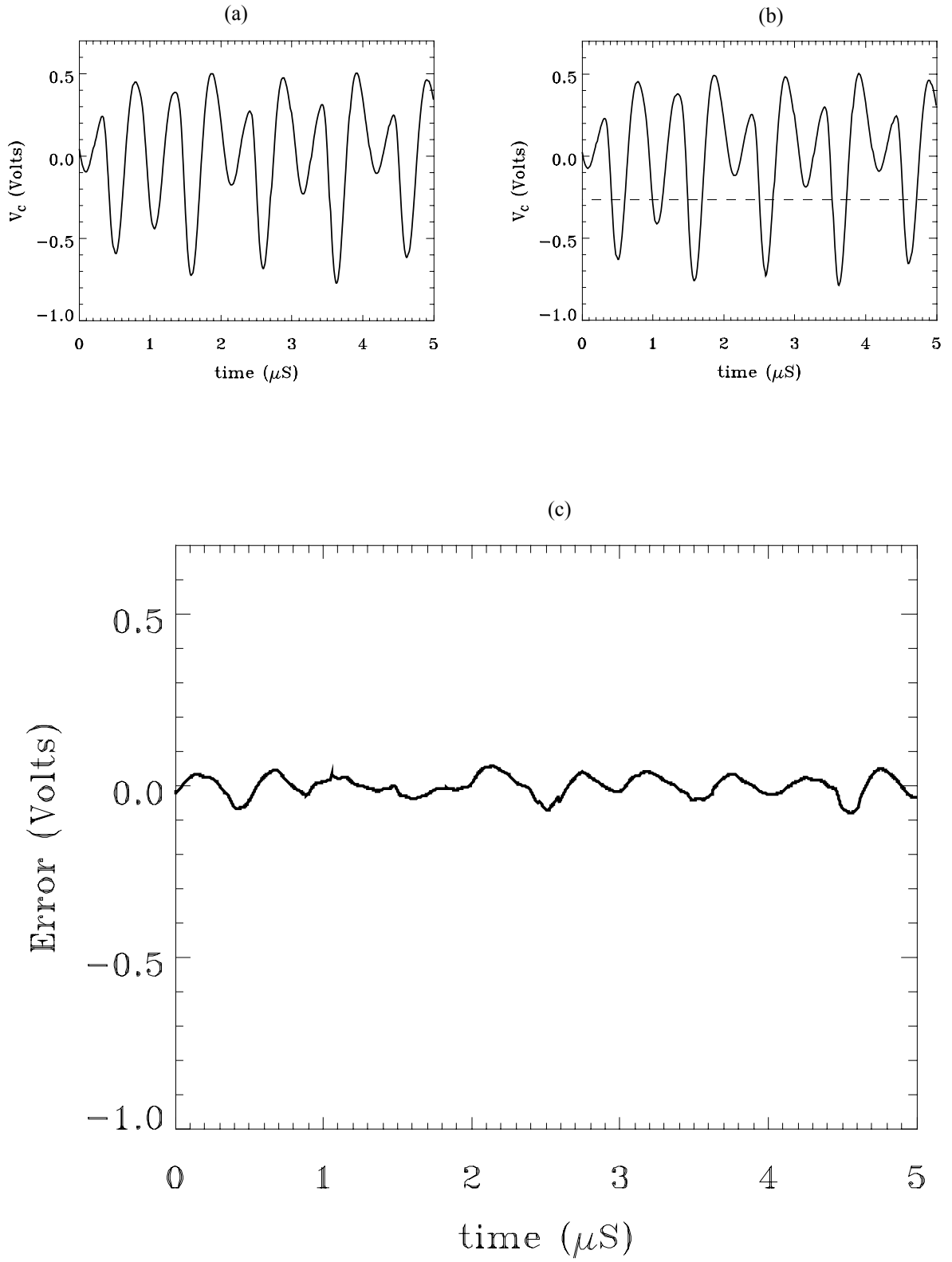


Fig. 3.11 Results from the 2 MHz syncrodyne amplifier circuit showing (a) the input signal, (b) the output signal and (c) the error signal.

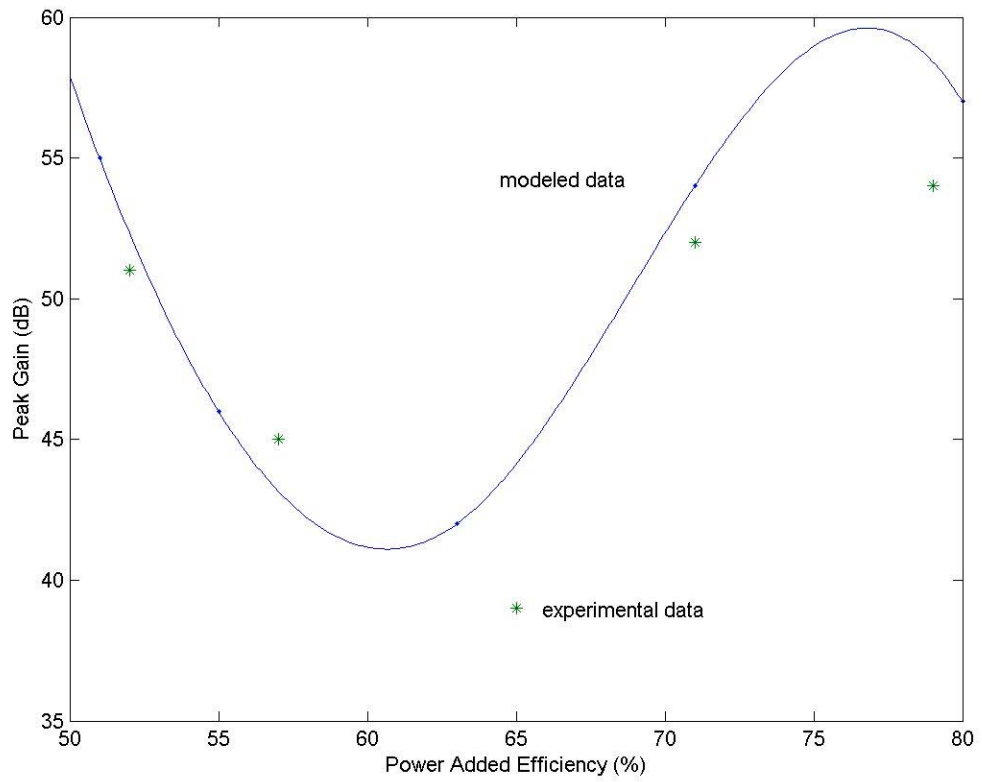


Figure 3.12 Comparison of experimental data from the 2 MHz syncrodyne amplifier with modeling results.

### 3.4 Preliminary Design of a 850 MHz Circuit

In order to suggest the feasibility of applying this technique to commercially viable communications systems we must show that it is possible to design such circuits at the frequencies of operation and have it capable of handling the types of signal formats used in them. A typical frequency band used in personal communications systems (PCS) is 824-850 MHz. Both CDMA and GSM, the dominate signal formats in the industry, are transmitted over this band [20].

The transistor we employ for this circuit is the heterojunction bipolar transistor (HBT). HBTs are the transistor of choice for high frequency applications because of its rapid response time and low source current requirements [23]. There is not a great deal of pre-packaged modeling information available for HBTs. Much of the work is still in the development stage. The model used in this circuit had to be derived from the manufacturer's specifications. Figure 3.13 shows the dc I-V characteristics for a specific HBT sample. This, along with other measured data from the manufacturers, was used to synthesis a reliable model for the transistor.

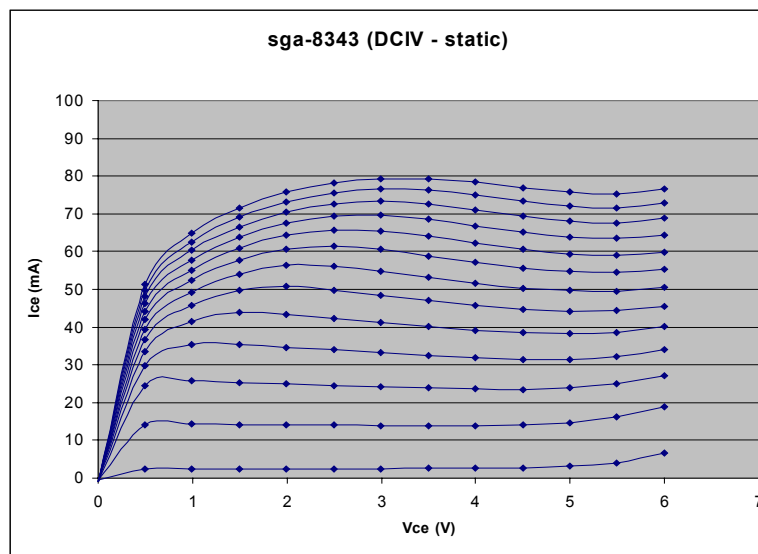


Figure 3.13 DC I-V characteristics for the high-frequency HBT used to model the 850 MHz circuit.

The circuit schematic diagram shown in figure 3.14 shows the Colpitts type circuit fashioned to implement a chaotic oscillator using this architecture. We have found that in the “search for chaos” the first, best place to start is the biasing structure supporting the transistor. Here  $R_1$  and  $R_b$  provide the first level of tuning to find regions of bounded instability. We attempted to keep  $V_{cc}$  around 3 V dc in order to be near the source voltages used in commercial practice.

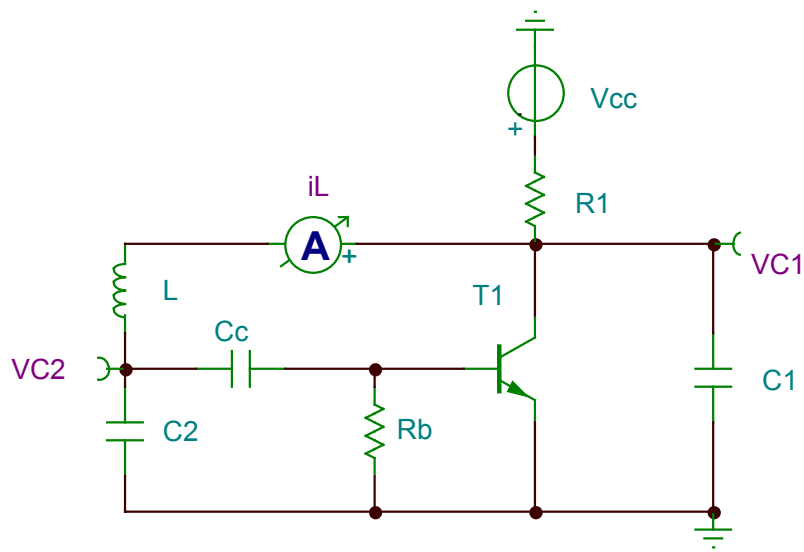


Figure 3.14 Schematic diagram of the high-frequency, Colpitts type, chaotic oscillator modeled using an HBT.

Figure 3.15 shows a time dependent oscillation of this slightly chaotic waveform. Note the variations in the valleys of the waveform. Again, restrictions on the ability to tune using the SPICE software limited our ability to find regions of highly chaotic motion. Our past experience tells us that a fabricated circuit will have more regions available for tuning. Figure 3.16 shows a two-dimensional projection of the state-space



using the inductor current and the voltage across  $C_2$  as variables. Note the slight fold that occurs in the trajectories. It can be argued that this is a 4-dimensional system (there are 4 independent variables) and that the chaotic attractor is higher than three dimensions. Finally, Figure 3.17 shows the frequency spectrum of the voltage across Capacitor 1. Its center frequency is about 836 MHz, which is center of the 824-850 MHz band.

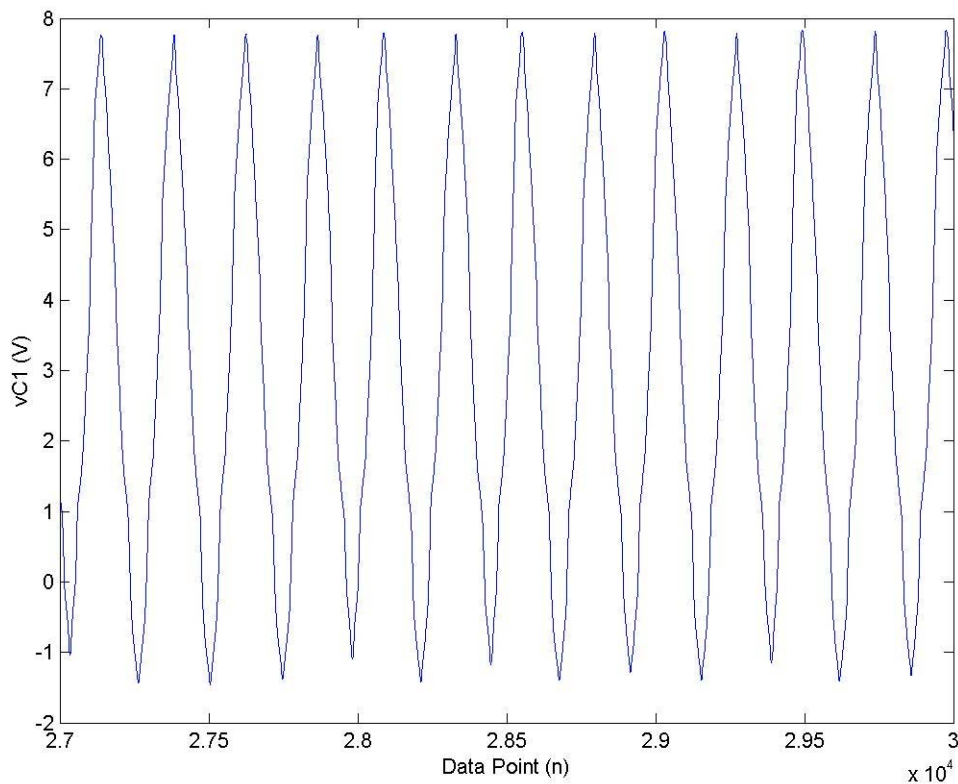


Figure 3.15 Time dependent oscillation of the voltage  $v_{C1}$  for the 850 MHz chaotic oscillator simulation.

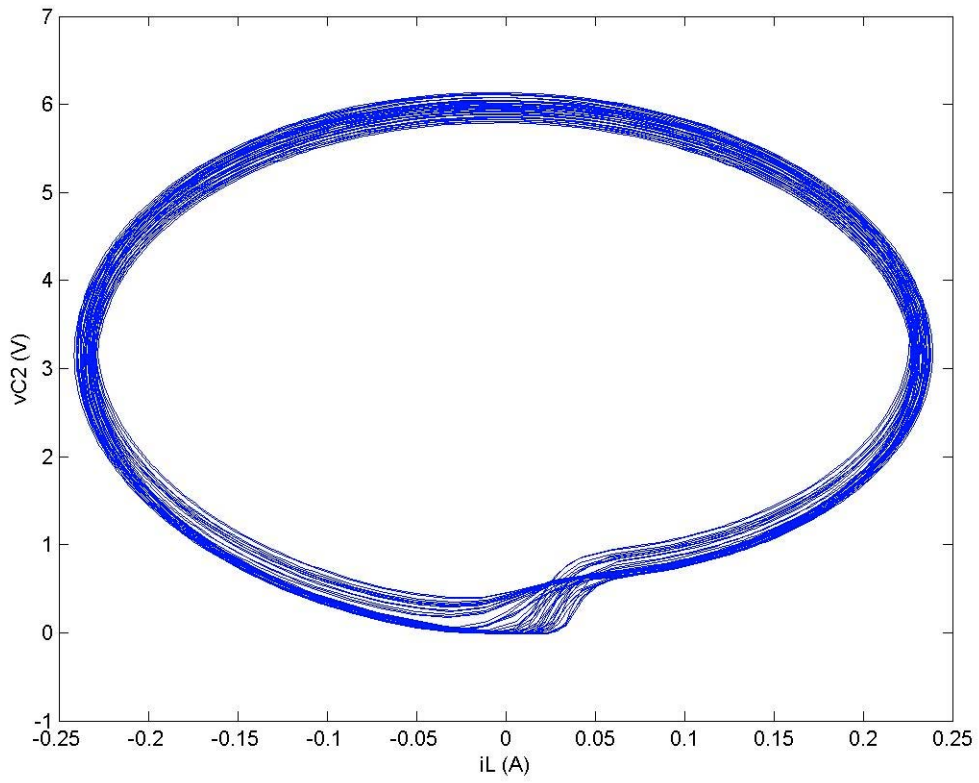


Figure 3.16 Two-dimensional projection of the state-space for the 850 MHz chaotic oscillator simulation.

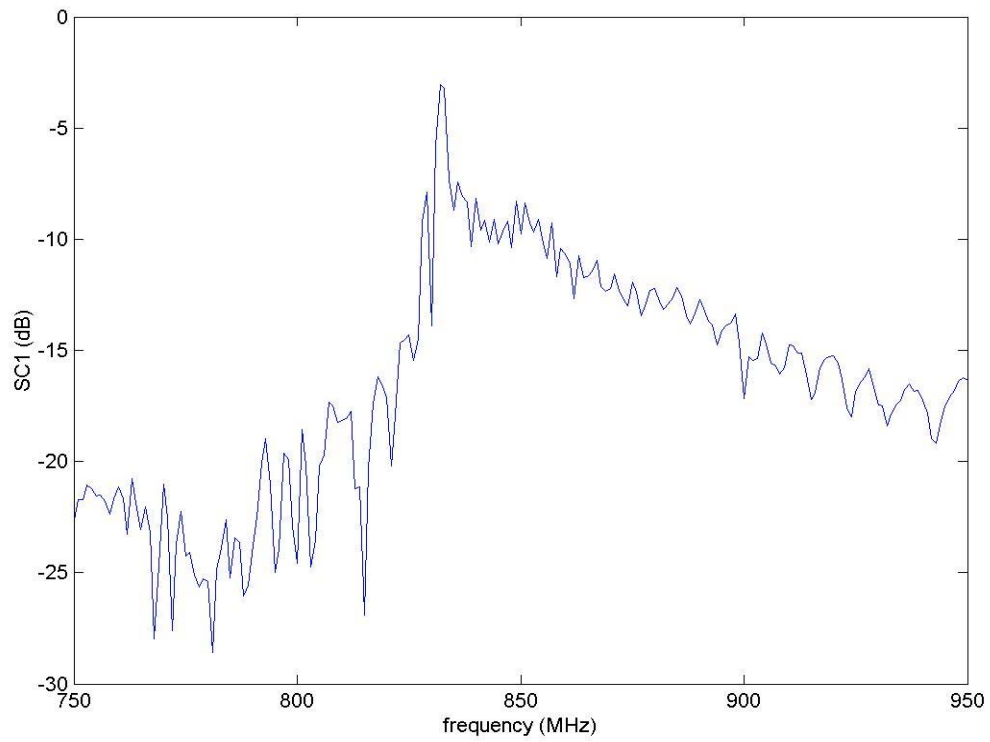


Figure 3.17 Frequency spectrum for the voltage across  $C_1$  for the 850 MHz chaotic oscillator simulation.

## CHAPTER 4

### Conclusion

#### 4.1 Discussion of Results

The purpose of this work was to demonstrate that a chaotic source could be synthesized that could be used to produce radio-frequency signals capable of carrying digital information. We began by showing that a discrete-time mapping called the logistic map, which is a basic, fundamental paradigm of chaotic behavior, is directly related to the Colpitts oscillator, which has been a cornerstone of communications technology for years. We were able to show that important measures of chaotic dynamics behavior, evident in the logistics map, were also present in mathematical models of the Colpitts oscillator. Further, we were able to show that it was possible to encode arbitrary binary information into the oscillations of the Colpitts circuit when in it was in a chaotic state, and it was also possible to achieve high-gain, high-efficiency power amplification of general communications signals such as CDMA and GSM, a process we've called *syncrodyne amplification*.

The mathematical model we derived was based upon the three-dimensional system of nonlinear differential equations that resulted from the Colpitts circuit. With it we showed how the synchronization property of chaotic systems was useful for syncrodyne amplification. We also were able to develop new relationships and measures such as the attractor volume and its relationship to the tuning parameter of the system. For the syncrodyne amplifier, we were able to show a functional relationship between the output power gain and the power added efficiency (PAE), demonstrating that nearly 60

dB gain and 80% PAE were possible. We were able to use the model to produce design tools which provide guidance in the fabrication of a circuit at 2 MHz.

We were successful in designing, laying out, fabricating and testing a chaotic oscillator that operated at 2 MHz. We used this circuit to empirically demonstrate the capability of encoding digital information directly into chaotic oscillations at about 1.67 Mbps. We also demonstrated a new method for power amplification called syncrodyne amplification. This circuit was able to provide over 40-dB power gain and over 72% power added efficiency.

Finally, we were able to detail some preliminary design criteria for a chaotic oscillator which operates in the 824-850 MHz band used in PCS applications. We used manufacturer specifications to derive a complete SPICE model for a heterojunction bipolar transistor (HBT) which acted as the nonlinear element in the circuit. We showed the resulting chaotic attractor, time waveforms, and the frequency spectrum of the output.

## 4.2 Implications

In response to customer demand manufacturers are introducing products capable of operating with higher speed 3G mobile services and adding new power hungry applications, such as wireless Internet, palm top computing, and integrating PDA and PCS functions. Battery life, which has been a principal concern of designers and end-users, will be further taxed by these feature rich handsets. A recent Frost & Sullivan report stated that current battery chemistries have reached their peak in their capabilities. Either new battery technologies must be produced now (which is unlikely) or there has to be more efficient use of the power provided. Without any improvement in battery life handset innovation will stagnate while demand continues to soar.

To solve this problem designers have concentrated on improving the efficiency of rf power amplifiers. Greater amplifier efficiency leads to simpler and less costly hand-held devices, increased battery life, and increased transmission speeds and distances. However, traditionally designed power amplifiers trade-off power gain or amplification for DC conversion efficiency and cannot yield the efficiency that the market requires. What is needed is a radical new approach to amplification. One that demonstrates dramatic improvement in not only power gain but conversion efficiency, signal distortion and power out capability. Nonlinear systems are inherently more efficient than linear systems. Chaotic systems are nonlinear systems that produce bounded instabilities that are being identified as beneficial for technological applications. Very high efficiency is also possible without signal distortion, because the Syncrodyne™ amplifier uses nonlinear dynamics in a natural way. The nonlinear operation is not an obstacle as it is in traditional designs, but is built into the way that the amplifier works from the start. The

demonstrated application of controlling symbolic dynamics for the encoding of digital information into chaotic oscillations, and the application of syncrodyne amplification for high-gain, high-efficiency power amplification is scalable in frequency, suggesting that devices operating well into the microwave frequency range and beyond are not far away.

In a general sense the introduction of bounded instability devices into the mainstream of technology applications and commercial engineering has the promise of improvements in a myriad of ways. More efficient devices are possible. Complex operations from very simple structures are possible. More importantly we are making the important step of taking these ideas beyond the confinements of research and thrusting them into the arena of engineering arts. In this work we've considered only a small piece of the possible areas of implementation, yet the potential impact on commercial technology can be huge.

Finally, we are optimistic about contributing to the general body of scientific and engineering knowledge. The promise of important applications and profitable industry impact can be a driver of increased study into this area of nonlinear dynamics, bounded instabilities, and their impact on technology. It is our intention to provide a basis for deeper investigation into this important phenomenon.

## APPENDIX A – MATLAB Procedures for Modeling and Analysis

*(All code is proprietary information and property of Syncrodyne Systems Corporation © 2002 All Rights*

*Reserved)*

### Colpitts Circuit Model Equations File (Colpitts.m)

```
function ds = Colpitts(Vcc,Vee,L,RL,C,Ce,Re,R,alpha,Bta,s)
% Function models a Colpitt's Oscillator
% A three dimensional set of nonlinear differential equations
% FUNCTION NAME: Colpitts.m
% INPUT: Vcc - collector voltage (Volts)
% INPUT: Vee - emitter voltage (Volts)
% INPUT: L - inductance (Henries)
% INPUT: RL - inductor resistance (Ohms)
% INPUT: C - capacitance (Farads)
% INPUT: Ce - emitter capacitance (Farads)
% INPUT: Re - emitter resistance (Ohms)
% INPUT: R - variable resistance (Ohms)
% INPUT: alpha - transistor exponential parameter (V^-1)
% INPUT: Beta - transistor multiplier parameter (A)
% INPUT: s - initial conditions [s(1),s(2),s(3)] = [iL,ve,vc]
% OUTPUT: ds - differential values (diL/dt,dve/dt,dvc/dt)
% DATE WRITTEN: December 21, 1999
% DATE MODIFIED: December 21, 1999
% PROGRAMMER: Chance M. Glenn, Director of Technology Development
% (c) 1999 NextWave Technologies, Inc.
% SYMDYNE TRANSMITTER Project
ds(1) = (Vcc-s(3)-(R+RL)*s(1))/L;           %iL
ds(2) = (s(1)-((s(2)-Vee)/Re))/Ce;       %Ve
ds(3) = (C*ds(2)+s(1)-ic(alpha,Bta,s(2)))/C; %Vc
```

### Colpitts Circuit Model Equations File for Synchronization (ColpittsSync.m)

```
function ds = ColpittsSync(Vcc,Vee,L,RL,C,Ce,Re,R,alpha,Bta,s,vC,RC)
% Function models a Colpitt's Oscillator
% A three dimensional set of nonlinear differential equations
% FUNCTION NAME: Colpitts.m
% INPUT: Vcc - collector voltage (Volts)
% INPUT: Vee - emitter voltage (Volts)
% INPUT: L - inductance (Henries)
% INPUT: RL - inductor resistance (Ohms)
% INPUT: C - capacitance (Farads)
% INPUT: Ce - emitter capacitance (Farads)
% INPUT: Re - emitter resistance (Ohms)
% INPUT: R - variable resistance (Ohms)
% INPUT: alpha - transistor exponential parameter (V^-1)
% INPUT: Beta - transistor multiplier parameter (A)
% INPUT: s - initial conditions [s(1),s(2),s(3)] = [iL,ve,vc]
% OUTPUT: ds - differential values (diL/dt,dve/dt,dvc/dt)
% DATE WRITTEN: December 21, 1999
% DATE MODIFIED: December 21, 1999
```

```

% PROGRAMMER: Chance M. Glenn, Director of Technology Development
% (c) 1999 NextWave Technologies, Inc.
% SYMDYNE TRANSMITTER Project
icouple = (vC-s(3))/RC; % Coupling
expression
ds(1) = (Vcc-s(3)-(R+RL)*s(1))/L; %iL
ds(2) = (s(1)-((s(2)-Vee)/Re))/Ce; %Ve
ds(3) = (C*ds(2)+s(1)-ic(alpha,Bta,s(2))+icouple)/C; %Vc

```

### Collector Current Equation for Transistor (iC.m)

```

function iout = iC(alpha,Bta,v)
% Function models the collector current for a
% 2N3904 transistor
% FUNCTION NAME: iC.m
% INPUT: alpha - transistor exponential parameter (V^-1)
% INPUT: Beta - transistor multiplier parameter (A)
% INPUT: v - input voltage (V)
% OUTPUT: iout - collector current (A)
% DATE WRITTEN: December 21, 1999
% DATE MODIFIED: December 21, 1999
% PROGRAMMER: Chance M. Glenn, Director of Technology Development
% (c) 1999 NextWave Technologies, Inc.
% SYMDYNE TRANSMITTER Project
iout = Bta *(exp(-alpha*v)-1.0);

```

### Euler Integration for Colpitts (Integrate\_C.m)

```

function sout =
INTEGRATE_C(Vcc,Vee,L,RL,C,Ce,Re,R,alpha,Bta,dt,Npts,s0)
for i = 1:Npts
    sout(1,i) = s0(1);
    sout(2,i) = s0(2);
    sout(3,i) = s0(3);
    s0 = s0 + dt*Colpitts(Vcc,Vee,L,RL,C,Ce,Re,R,alpha,Bta,s0);
end

```

### Euler Integration for Synchronized Colpitts (Integrate\_CSync.m)

```

function sout =
INTEGRATE_CSync(Vcc,Vee,L,RL,C,Ce,Re,R,alpha,Bta,dt,Npts,s0)
for i = 1:Npts
    sout(1,i) = s0(1);
    sout(2,i) = s0(2);
    sout(3,i) = s0(3);
    s0 = s0 + dt*Colpitts(Vcc,Vee,L,RL,C,Ce,Re,R,alpha,Bta,s0);
end

```



## Poincaré Surface of Section Calculation (PSSCHK.m)

```

% Function that checks for and returns the Poincare surface of
% section coordinates
% s0 - data point 0
% s - next data point
% PSSD - Poincare surface coordinates [3,2]
%           1-x,2-y,3-z ,1-x0,2-xf
function PSSout = PSSCHK(s0,s,PSSD)
PSSout = [0.0;0.0;0.0];
if PSSD(1,1) == PSSD(1,2) % Constant X surface
    if ((s(1)<=PSSD(1,1)) & (s0(1)>=PSSD(1,2)))
        pssX = INTERP(s0(1),s(1),s0(2),s(2),PSSD(1,1));
        pssY = INTERP(s0(1),s(1),s0(3),s(3),PSSD(1,1));
        if
            (pssX>=PSSD(2,1)) & (pssX<=PSSD(2,2)) & (pssY>=PSSD(3,1)) & (pssY<=PSSD(3,2))
                PSSout(1) = 1.0;
                PSSout(2) = pssX;
                PSSout(3) = pssY;
            end
        end
        if ((s(1)>=PSSD(1,1)) & (s0(1)<=PSSD(1,2)))
            pssX = INTERP(s0(1),s(1),s0(2),s(2),PSSD(1,1));
            pssY = INTERP(s0(1),s(1),s0(3),s(3),PSSD(1,1));
            if
                (pssX>=PSSD(2,1)) & (pssX<=PSSD(2,2)) & (pssY>=PSSD(3,1)) & (pssY<=PSSD(3,2))
                    PSSout(1) = 1.0;
                    PSSout(2) = pssX;
                    PSSout(3) = pssY;
                end
            end
        end
    end
if PSSD(2,1) == PSSD(2,2) % Constant Y surface
    if ((s(2)<=PSSD(2,1)) & (s0(2)>=PSSD(2,2)))
        pssX = INTERP(s0(2),s(2),s0(1),s(1),PSSD(2,1));
        pssY = INTERP(s0(2),s(2),s0(3),s(3),PSSD(2,1));
        if
            (pssX>=PSSD(1,1)) & (pssX<=PSSD(1,2)) & (pssY>=PSSD(3,1)) & (pssY<=PSSD(3,2))
                PSSout(1) = 1.0;
                PSSout(2) = pssX;
                PSSout(3) = pssY;
            end
        end
        if ((s(2)>=PSSD(2,1)) & (s0(2)<=PSSD(2,2)))
            pssX = INTERP(s0(2),s(2),s0(1),s(1),PSSD(2,1));
            pssY = INTERP(s0(2),s(2),s0(3),s(3),PSSD(2,1));
            if
                (pssX>=PSSD(1,1)) & (pssX<=PSSD(1,2)) & (pssY>=PSSD(3,1)) & (pssY<=PSSD(3,2))
                    PSSout(1) = 1.0;
                    PSSout(2) = pssX;
                    PSSout(3) = pssY;
                end
            end
        end
    end
if PSSD(3,1) == PSSD(3,2) % Constant Z surface

```

```

    if ((s(3) <= PSSD(3,1)) & (s0(3) >= PSSD(3,2)))
        pssX = INTERP(s0(3), s(3), s0(1), s(1), PSSD(3,1));
        pssY = INTERP(s0(3), s(3), s0(2), s(2), PSSD(3,1));
        if
            (pssX >= PSSD(1,1)) & (pssX <= PSSD(1,2)) & (pssY >= PSSD(2,1)) & (pssY <= PSSD(2,2))
                PSSout(1) = 1.0;
                PSSout(2) = pssX;
                PSSout(3) = pssY;
            end
        end
    if ((s(3) >= PSSD(3,1)) & (s0(3) <= PSSD(3,2)))
        pssX = INTERP(s0(3), s(3), s0(1), s(1), PSSD(3,1));
        pssY = INTERP(s0(3), s(3), s0(2), s(2), PSSD(3,1));
        if
            (pssX >= PSSD(1,1)) & (pssX <= PSSD(1,2)) & (pssY >= PSSD(2,1)) & (pssY <= PSSD(2,2))
                PSSout(1) = 1.0;
                PSSout(2) = pssX;
                PSSout(3) = pssY;
            end
        end
    end
end

```

### Poincaré Surface Point Gathering (GETPSS.m)

```

function pssV = GETPSS(s, PSS, Npts)
psscoun = 0;
for i = 2:Npts
    PSSout = PSSCHK(s(:,i-1), s(:,i), PSS);
    if PSSout(1) == 1.0
        psscoun = psscoun + 1;
        pssV(1,psscoun) = PSSout(2);
        pssV(2,psscoun) = PSSout(3);
    end
end
end

```

### Interpolation Routine for Poincaré Surface (INTERP.m)

```

% Linear Interpolation function (x1,x2,y1,y2,x)
function y = INTERP(x1,x2,y1,y2,x)
m = (y1-y2)/(x1-x2);
b = (x1*y2-x2*y1)/(x1-x2);
y = m*x + b;

```

### Syncrodyne Simulation Procedure (Syncrodyne\_SIM.m)

```

% Script file that simulate a Colpitts Oscillator Simulation run.
% Uses Colpitts Oscillator
% Filename: Syncrodyne_SIM.m ver 2.0
% Date Created: August 12, 1999
% Date Modified: November 6, 2001

```

```

clear
% 1.0 MODEL PARAMETER DEFINITION
Cbase = 1750.0e-12;
dC = 100.0e-12;
Cadd = 50.0e-12;
C = Cbase+Cadd;
Ce = C;

Re = 400.0;
Vcc = 5.00;
Vee = -5.00;

L = 6.8e-6;
RL = 2.0;

Rbase = 50.00;
dR = 50;
Radd = 0.00;
R = Rbase+Radd;

dRCon = 11.0;
RConbase = 1.0;
RConadd = 4.0;
RCon = RConbase+RConadd;
RCoff = 2e50;

Nmag = 1e-10;

% 1.1 BJT PARAMETER DEFINITION
alpha = 41.2;
Bta = 1.06e-15;
% 1.2 SIMULATION PARAMETERS
dt = 4.0e-09; % seconds
t0 = 0.0; % seconds
s01 = [0.0030 -0.6594 10.0496];
s02 = [0.042 0.7337, 9.5259];
s01 = [0.0 0.0 0.0];
s02 = [0.0 0.0 0.0];
fin = 1.8e6;
pi = 3.1415926537;

dfin = 0.6e6;
finbase = 1.5e6;
finadd = 0.3e6;
fin = finbase+finadd;
win = 2.0*pi*fin;

dA = 2.0;
Abase = 0.1;
Aadd = 0.9;
A = Abase+Aadd;

dAdc = 1.0;
Adcbase = -0.5;
Adcadd = 0.5;
Adc = Adcbase+Adcadd;

```

```

%      1.3 OUPUT TIME WINDOW DEFINITION
wlength = 512;
t0 = 0.0;
tmax = dt*(wlength-1);
t = t0:dt:tmax;
xopw = (1:wlength)*0.0;
xipw = xopw;
xerrw = (1:wlength)*0.0;
Vcmin = -15.0;
Vcmax = 15;
Vemin = -4.0;
Vemax = 10.0;
iLmin = -0.05;
iLmax = 0.2;
errmin = -0.5;
errmax = 0.5;
% 1.4 FREQUENCY DEFINITION
fmax = 1/dt;
f0 = 0.0;
ff = 5e6;
Nf = 10*wlength;
df = (fmax-f0)/(Nf-1);
f = f0:df:fmax;
Dfreq = 500;
freqw = abs(fft(xopw,Nf))/Dfreq;
syncflag = -1;

% 2.0 SET UP AXES
h = get(gcf,'Children');
% h(30) error waveform, h(31) state space, h(32) frequency,
% h(33) input, h(34) output
%      2.1 OUTPUT TIME WINDOW
subplot(h(34))
pxopw = plot(t,xopw,'EraseMode','xor');
axis([t0 tmax Vemin Vemax])
xlabel('time (sec)')
ylabel('Ve (V)')
% 2.2 INPUT TIME WINDOW
subplot(h(33))
pxipw = plot(t,xipw,'EraseMode','xor');
axis([t0 tmax Vemin Vemax])
xlabel('time (sec)')
ylabel('Ve (V)')
% 2.3 ERROR TIME WINDOW
subplot(h(30))
pxerrw = plot(t,xerrw,'EraseMode','xor');
axis([t0 tmax errmin errmax])
xlabel('time (sec)')
ylabel('Verr (V)')
% 2.4 FREQUENCY WAVEFORMS
subplot(h(32))
pfreqw = plot(f,freqw,'EraseMode','xor');
axis([f0 ff 0 1])
xlabel('frequency (Hz)')
ylabel('V/Hz (normalized)')

```

```

% 2.5 STATE-SPACE WINDOW
subplot(h(31))
xsnaek = s01(1)+(1:wlength/10)*0.0;
ysnaek = s01(2)+(1:wlength/10)*0.0;
zsnaek = s01(3)+(1:wlength/10)*0.0;
pssw =
plot3(s01(1),s01(2),s01(3),'c.','MarkerSize',2,'EraseMode','none');
hold on
psnaek = plot3(xsnaek,ysnaek,zsnaek,'b','EraseMode','xor');
psnaeker = plot3(xsnaek,ysnaek,zsnaek,'w','EraseMode','xor');
axis([iLmin iLmax Vemin Vemax Vcmin Vcmax])
xlabel('iL (A)')
ylabel('Ve (V)')
zlabel('Vc (V)')
hold off

runflag = 1;
pauseflag = 0;
tA = 0.0;
sigValue = 1;

% 2.6 POWER CALCULATION INITIALIZATION
PLsum = 0.0;
PRLsum = 0.0;
PRsum = 0.0;
PQsum = 0.0;
PCsum = 0.0;
PCesum = 0.0;
PRCsum = 0.0;
Poutsum = 0.0;
Pinsum = 0.0;
Peesum = 0.0;
Pccsum = 0.0;

ncalc = 1;

% 3.0 CALCULATE DATA
while runflag == 1
    R = Rbase+Radd;
    C = Cbase+Cadd;
    Ce = C;
    A = Abase+Aadd;
    Adc = Adcbase+Adcadd;
    fin = finbase+finadd;
    win = 2.0*pi*fin;
    if (sigValue == 1)
        vC = Adc+A*s02(2);
        s02 = s02 + dt*Colpitts(Vcc,Vee,L,RL,C,Ce,Re,R,alpha,Bta,s02);
        s02(1) = s02(1) + NOISE(Nmag);
        s02(2) = s02(2) + NOISE(Nmag);
        s02(3) = s02(3) + NOISE(Nmag);
    elseif (sigValue == 2)
        vC = Adc+A*sin(win*tA);
    end
    RCon = RConbase+RConadd;

```

```

if syncflag == -1
    RC = RCoff;
else
    RC = RCon;
end

AHndl = findobj(gcbf, 'Tag', 'StaticText22');
set(AHndl, 'String', sprintf('%5.2f', A));
AdcHndl = findobj(gcbf, 'Tag', 'StaticText23');
set(AdcHndl, 'String', sprintf('%6.3f', Adc));
freqHndl = findobj(gcbf, 'Tag', 'StaticText24');
set(freqHndl, 'String', sprintf('%6.3f', fin/1e6));

Vs = ColpittsSync2(Vcc, Vee, L, RL, C, Ce, Re, R, alpha, Bta, s01, vC, RC);
s01 = s01 + dt*Vs;
s01(1) = s01(1) + NOISE(Nmag);
s01(2) = s01(2) + NOISE(Nmag);
s01(3) = s01(3) + NOISE(Nmag);
xsnake = XSHIFT(xsnake, s01(1));
ysnake = XSHIFT(ysnake, s01(2));
zsnake = XSHIFT(zsnake, s01(3));
err = vC-s01(2);
xopw = XSHIFT(xopw, s01(2));
xipw = XSHIFT(xipw, vC);

% 3.1 ERROR/POWER/GAIN/EFFICIENCY CALCULATIONS
% 3.1.1 RMS DISTORTION
xerrw = XSHIFT(xerrw, err);
rmsdist =
100.0*(sum(xerrw.*xerrw)/wlength)/(sum(xipw.*xipw)/wlength);
rmsHndl = findobj(gcbf, 'Tag', 'StaticText14');
set(rmsHndl, 'String', sprintf('%6.3f', rmsdist))
% 3.1.2 POWER GAIN
Poutsum = Poutsum + ((s01(2)-Vee)*(s01(2)-Vee))/Re;
Pout = Poutsum/ncalc;
PoutdBm = 10.0*log10(Pout/0.001);
Pinsum = Pinsum + err*vC/RC;
Pin = Pinsum/ncalc;
Gain = 10.0*log10(Pout/Pin);
gnHndl = findobj(gcbf, 'Tag', 'StaticText12');
set(gnHndl, 'String', sprintf('%5.2f', Gain))
PoHndl = findobj(gcbf, 'Tag', 'StaticText19');
set(PoHndl, 'String', sprintf('%6.2f', PoutdBm));

% 3.1.3 CONVERSION EFFICIENCY/POWER ADDED EFFICIENCY
PLsum = PLsum + s01(1)*L*Vs(1);
PL = PLsum/ncalc;
PRLsum = PRLsum + RL*s01(1)*s01(1);
PRL = PRLsum/ncalc;
PRsum = PRsum + R*s01(1)*s01(1);
PR = PRsum/ncalc;
PQsum = PQsum + (s01(1)-C*(Vs(3)-Vs(2)))*(s01(3)-s01(2));
PQ = PQsum/ncalc;
PCsum = PCsum + (s01(3)-s01(2))*C*Vs(3);
PC = PCsum/ncalc;
PCesum = PCesum + s01(3)*Ce*Vs(2);

```

```

PCe = PCesum/ncalc;
PRCsum = PRCsum + err*err/RC;
PRC = PRCsum/ncalc;
Pccsum = Pccsum + Vcc*s01(1);
Pcc = Pccsum/ncalc;
Peesum = Peesum + Vee*(s01(2)-Vee)/Re;
Pee = Peesum/ncalc;
Ptot = PL+PRL+PR+PQ+PC+PCe+Pout+PRC;
Ptot2 = Pcc+Pee+PRC;
PCE = 100.0*(Pout/Ptot);
PAE = 100.0*((Pout-Pin)/Ptot);
PCEHndl = findobj(gcbf,'Tag','StaticText13');
set(PCEHndl,'String',sprintf('%5.2f',PCE));
PAEHndl = findobj(gcbf,'Tag','StaticText20');
set(PAEHndl,'String',sprintf('%5.2f',PAE));

RHndl = findobj(gcbf,'Tag','StaticText9');
set(RHndl,'String',sprintf('%5.2f',R))
CHndl = findobj(gcbf,'Tag','StaticText10');
set(CHndl,'String',sprintf('%5.2f',C/1e-9))
RCHndl = findobj(gcbf,'Tag','StaticText16');
set(RCHndl,'String',sprintf('%5.2e',RC))

freqw = abs(fft(xopw,Nf))/Dfreq;
set(pxopw,'XData',t,'YData',xopw)
set(pxipw,'XData',t,'YData',xipw)
set(pxerrw,'XData',t,'YData',xerrw)
set(pfreqw,'XData',f,'YData',freqw)
set(pssw,'XData',s01(1),'YData',s01(2),'ZData',s01(3))
set(psnake,'XData',xsnake,'YData',ysnake,'ZData',zsnake)
set(psnakeer,'XData',xsnake,'YData',ysnake,'ZData',zsnake)
drawnow

tA = tA + dt;
ncalc = ncalc + 1;
end

```

## GSM and CDMA Waveform Generation (GENERATE\_WAVEFORMS.m)

```

% FILENAME: GENERATE_WAVEFORMS.m
% DESCRIPTION: A test and analysis procedure that generates
%             CMDA (QPSK), OQPSK and GSM (GMSK) waveforms
%             for analysis and for testing with the Syncrodyne
%             Amplifier series-3 prototype.
%
% PROJECT: Syncrodyne Amplifier Series-3 Prototype
%          (c) 2002 Syncrodyne Systems Corporation
%          Chance M. Glenn, Sr. - Project Manager, programmer
% DATE BEGAN: July 19, 2002
% DATE MODIFIED: July 24, 2002

clear

% 1.0 INITIALIZATION

```

```

% 1.1 GENERAL
pi = 3.1415926537; % pi
fc = 836.5e6; % Carrier frequency (Hz)
fc = 2e6;
B = '1010110111011110'; % Random input bit sequence
B = '11000111';
NB = length(B); % Length of bit sequence
nppc_c = 32; % Number of points per
cycle for carrier
Tc = 1.0/fc; % Carrier period (sec)
dt = Tc/nppc_c; % Time step (sec)

% 1.2 CDMA
brCDMA = 1.2288e6; % CDMA bit (chip) rate
(bps)
T_CDMA = 1.0/brCDMA; % CDMA bit period (sec)
nppb_CDMA = T_CDMA/dt; % Number of points per bit
(CDMA)

% 1.3 GSM
brGSM = 270.8e3; % GSM bit rate (bps)
brGSM = 650.0;
T_GSM = 1.0/brGSM; % GSM bit period (sec)
nppb_GSM = T_GSM/dt; % Number of points per bit
(GSM)
BT = 0.3; % Gaussian product factor
BG = BT/T_GSM; % 3-dB bandwidth of
gaussian filter
mGMSK = sqrt(log(2))/sqrt(2); % Gaussian shaping factor
a_GSM = mGMSK/BG; % GMSK premodulation index

% 2.0 GENERATE WAVEFORMS
% 2.1 BASEBAND SIGNALS
% 2.1.1 CDMA
%dCDMA = dIQ(B,nppb_CDMA); % I and Q baseband
components
%tCDMA = dt*(0:length(dCDMA)-1); % Time array (CDMA)
%tmax_CDMA = max(tCDMA); % Maximum time (CDMA)
% 2.1.2 GSM
dGSM = dIQHS(B,nppb_GSM); % I and Q baseband
components using half-sine
dGSM = QPSK2QPSK(dGSM,nppb_GSM); % Offset QPSK shifting
tGSM = dt*(0:length(dGSM)-1); % Time array (GSM)
tmax_GSM = max(tGSM); % Maximum time (GSM)
% 2.1.2.1 GAUSSIAN FILTERING GSM BASEBAND
fmax = 1/dt; % Maximum frequency
df_GSM = fmax/(length(dGSM(1,:))-1); % Frequency step
f_GSM = 0:df_GSM:fmax; % Frequency array (GSM)
HGMSK = GPF(a_GSM,f_GSM); % GMSK transfer function
fd_GSMI = fft(dGSM(1,:)); % Fourier transform of In-
phase component
fd_GSMQ = fft(dGSM(2,:)); % Fourier transform of
Quadrature component
fd_GSMI_H = fd_GSMI.*HGMSK; % Filtering multiplication
(I)

```



```

fd_GSMQ_H = fd_GSMQ.*HGMSK;           % Filtering multiplication
(Q)
dGSMH(1,:) = real(iffd(fd_GSMI_H));    % Inverse transformation
(I)
dGSMH(2,:) = real(iffd(fd_GSMQ_H));    % Inverse transformation
(Q)

% 2.2 MODULATE CARRIER
wc = 2.0*pi*fc;                       % Carrier radian frequency
(radians/s)
A = 1.0/sqrt(2.0);                    % Constant multiplier
% 2.2.2 GSM MODULATION
sI_GSM = A*dGSM(1,:).*cos(wc*tGSM+pi/4.0); % In-phase modulation
component
sQ_GSM = A*dGSM(2,:).*sin(wc*tGSM+pi/4.0); % Quadrature modulation
component
s_GSM = sI_GSM+sQ_GSM;                % Combined waveform
fs_GSM = fft(s_GSM);                  % Frequency spectra

% 3.0 PLOTS

% 3.3 GSM BASEBAND WAVEFORMS
% 3.3.1 IN-PHASE
figure(5)
plot(tGSM/1e-3,dGSMH(1,:))
xlabel('time (msec)')
ylabel('In-phase Component')
title('GSM Baseband In-phase Bit-stream')
% 3.3.1 QUADRATURE
figure(6)
plot(tGSM/1e-3,dGSMH(2,:))
xlabel('time (msec)')
ylabel('In-phase Component')
title('GSM Baseband Quadrature Bit-stream')

% 3.4 GSM MODULATED CARRIER
% 3.4.1 TIME WAVEFORM
figure(7)
plot(tGSM/1e-3,s_GSM);
axis([0.52 0.525 -0.75 0.75])
xlabel('time (msec)')
ylabel('s(t)')
title('GSM Modulated Carrier')
% 3.4.2 FREQUENCY SPECTRA
figure(8)
plot(f_GSM/1e6,20.0*log10(abs(fs_GSM)/length(fs_GSM)))
axis([1.8 2.2 -120 -10.0])
xlabel('frequency (MHz)')
ylabel('Power Spectra (dB)')

```

## In-Phase and Quadrature Component Generation (dIQ.m & dIQHS.m)

```

function dIQout = dIQ(B,nppb)
% FILENAME: dIQ.m

```

```

% DESCRIPTION: Generates the in-phase and quadrature bit-stream
%               components for a given bit sequence. Assumes an even
%               number of bits.
% INPUT: B - character array representing input bit sequence
%         nppb - number of points per bit
% OUTPUT: dIQout - two dimensional array of
%           nB/2 (number of bits) x nppb data points representing
%           in-phase and quadrature components
%           dIQ(1,:) - in-phase
%           dIQ(2,:) - quadrature
% PROJECT: Syncrodyne Amplifier Series-3 Prototype
%           (c) 2002 Syncrodyne Systems Corporation
%           Chance M. Glenn, Sr. - Project Manager, programmer
% DATE BEGAN: July 18, 2002
% DATE MODIFIED: July 18, 2002

NB = length(B);
dbase = 1.0+(1:nppb)*0.0;

% 1.0 INITIAL TWO BITS
% 1.1 IN-PHASE
if B(1) == '0'
    dI = -dbase;           % bit zero, -
else
    dI = dbase;           % bit one, +
end
% 1.2 QUADRATURE
if B(2) == '0'
    dQ = -dbase;           % bit zero, -
else
    dQ = dbase;           % bit one, +
end

% 2.0 REMAINING BITS
for i = 3:NB
    if i/2 == fix(i/2)     % even QUADRATURE
        if B(i) == '0'
            dQ = [dQ,-dbase];           % bit zero, -
        else
            dQ = [dQ,dbase];           % bit one, +
        end
    else                   % odd IN-PHASE
        if B(i) == '0'
            dI = [dI,-dbase];           % bit zero, -
        else
            dI = [dI,dbase];           % bit one, +
        end
    end
end

%3.0 OUTPUT
dIQout(1,:) = dI;
dIQout(2,:) = dQ;

```

```

function dIQout = dIQHS(B,nppb)
% FILENAME: dIQHS.m
% DESCRIPTION: Generates the in-phase and quadrature bit-stream
%               components for a given bit sequence using
%               half-sines as the basis. Assumes an even
%               number of bits.
% INPUT: B - character array representing input bit sequence
%         nppb - number of points per bit
% OUTPUT: dIQout - two dimensional array of
%           nB/2 (number of bits) x nppb data points representing
%           in-phase and quadrature components
%           dIQ(1,:) - in-phase
%           dIQ(2,:) - quadrature
% PROJECT: Syncrodyne Amplifier Series-3 Prototype
%           (c) 2002 Syncrodyne Systems Corporation
%           Chance M. Glenn, Sr. - Project Manager, programmer
% DATE BEGAN: July 19, 2002
% DATE MODIFIED: July 19, 2002

NB = length(B);
dbase = halvesine(nppb);

% 1.0 INITIAL TWO BITS
% 1.1 IN-PHASE
if B(1) == '0'
    dI = -dbase;           % bit zero, -
else
    dI = dbase;           % bit one, +
end
% 1.2 QUADRATURE
if B(2) == '0'
    dQ = -dbase;           % bit zero, -
else
    dQ = dbase;           % bit one, +
end

% 2.0 REMAINING BITS
for i = 3:NB
    if i/2 == fix(i/2)     % even QUADRATURE
        if B(i) == '0'
            dQ = [dQ,-dbase];           % bit zero, -
        else
            dQ = [dQ,dbase];           % bit one, +
        end
    else                   % odd IN-PHASE
        if B(i) == '0'
            dI = [dI,-dbase];           % bit zero, -
        else
            dI = [dI,dbase];           % bit one, +
        end
    end
end

%3.0 OUTPUT
dIQout(1,:) = dI;
dIQout(2,:) = dQ;

```

## QPSK to Offset-QPSK Transformation (QPSK2OQPSK.m)

```
function dIQout = QPSK2OQPSK(dIQ,nppb)
% FILENAME: QPSK2OQPSK.m
% DESCRIPTION: Turns a QPSK baseband bit-stream waveform into
%               a OQPSK waveform by shifting the quadrature
%               component by a half-bit time.
% INPUT:      dIQ - two-dimensional array containing original
%               I and Q bit stream
%               nppb - number of points per bit
% OUTPUT:    dIQout - two-dimensional array of containing the
%               shifted waveform. 1-I, 2-Q
% PROJECT:   Syncrodyne Amplifier Series-3 Prototype
%           (c) 2002 Syncrodyne Systems Corporation
%           Chance M. Glenn, Sr. - Project Manager, programmer
% DATE BEGAN: July 19, 2002
% DATE MODIFIED: July 19, 2002

dadd = 0.0*(1:nppb/2);
dI = [dIQ(1,:),dadd];
dQ = [dadd,dIQ(2,:)];
dIQout(1,:) = dI;
dIQout(2,:) = dQ;
```

## Generate GMSK Waveform (GENERATE\_GMSK.m)

```
% FILENAME: GENERATE_GMSK.m
% DESCRIPTION: Procedure for generating a GMSK Waveform
%
% PROJECT: Phase 3 Syncrodyne Amplifier Prototype
%           0.3 GMSK 1875 MHz (PCS1900)
%           (c) 2002 Syncrodyne Systems Corporation
%           All Rights Reserved
%
% PROGRAMMER: Chance M. Glenn
% DATE BEGAN: March 19, 2002
% DATE MODIFIED: March 19, 2002

% INPUT PARAMETERS
pi = 3.1415926537; % pi
BT = 0.3; % Gaussian product factor
Rb = 270.833e3; % Bit Rate
Tb = 1.0/Rb;
BG = BT/Tb;
a = sqrt(log(2))/(sqrt(2)*BG); % GMSK premodulation index
ppb = 100; % Time points per bit
dt = Tb/ppb; % Time step
B = [1,1,0,0,1,1,1,0,0,1,0,0,1,0,1,0,1,1,1,0,0,0,1,0]; % Bit sequence
NB = length(B); % Number of bits in bits
sequence
Tmax = Tb*NB; % Maximum time
```

```

fc = 1875.0e6; % Carrier frequency

t = 0:dt:Tmax-dt;
SMSK = 0.0*t;

mI = mI_GMSK(dt,B,Rb);
mQ = mQ_GMSK(dt,B,Rb);
for i = 1:NB
    for j = 1:length(t)
        c(j) = cos(2.0*pi*fc*t(j));
        s(j) = sin(2.0*pi*fc*t(j));
        pc(j) = pGMSK(t(j)-2*(i-1)*Tb,Tb);
        ps(j) = pGMSK(t(j)-2*(i-1)*Tb-Tb,Tb);
        cpc(j) = mI(j)*c(j)*pc(j);
        sps(j) = mQ(j)*s(j)*ps(j);
    end
    SMSK = SMSK + cpc + sps;
end

```

## S-Parameters to ABCD Parameter Transformation (S2ABCD.m)

```

function Aout = S2ABCD(s11,s12,s21,s22,Z0)
% FILENAME: S2ABCD.m
% DESCRIPTION: Function that converts S-parameters to ABCD
%               matrix parameters
% INPUT: s11 - out port 1 incident on port 1
%        s12 - out port 1 incident on port 2
%        s21 - out port 2 incident on port 1
%        s22 - out port 2 incident on port 2
% OUTPUT: Aout - ABCD Matrix (1-A,2-B,3-C,4-D)
% PROJECT: Synrodyne Amplifier Series-3 Prototype
%          (c) 2002 Synrodyne Systems Corporation
%          Chance M. Glenn, Sr. - Project Manager, programmer
%          REFERENCE: Wolff,Kaul - "Microwave Engineering and Systems
%          Applications"
% DATE BEGAN: August 28, 2002
% DATE MODIFIED: August 28, 2002

Y0 = 1/Z0;
M = 1/(2*s21);
A = M*((1+s11)*(1-s22)+s12*s21);
B = M*Z0*((1-s11)*(1+s22)-s12*s21);
C = M*Y0*((1-s11)*(1-s22)-s12*s21);
D = M*((1-s11)*(1+s22)+s12*s21);
Aout(1) = A;
Aout(2) = B;
Aout(3) = C;
Aout(4) = D;

```

## HBT Analysis Procedure (HBT\_ANALYSIS.m)

```
% FILENAME: HBT_ANALYSIS.m
% DESCRIPTION: .
%
% PROJECT: Syncrodyne Amplifier Series-3 Prototype
%           (c) 2002 Syncrodyne Systems Corporation
%           Chance M. Glenn, Sr. - Project Manager, programmer
% DATE BEGAN: August 28, 2002
% DATE MODIFIED: August 28, 2002

clear

% 1.0 PARAMETER DEFINITION
pi = 3.1415926537;
f0 = 850.0e6; % Measurement frequency (Hz)
w0 = 2.0*pi*f0; % Radian frequency (rad/s)
Z0 = 50.0; % Input/Output Impedance (Ohms)

% 1.1 OPERATING POINT #1
V1 = 2.0; % Operating point voltage #1 (V)
I1 = 10.0e-3; % Operating point current #1 (A)
s11_1 = -0.09638-j*0.52828;
s12_1 = 0.030119+j*0.400359;
s21_1 = -4.414662+j*11.899266;
s22_1 = 0.375207-j*0.4374132;
A1 = S2ABCD(s11_1,s12_1,s21_1,s22_1,Z0);
XC1 = abs(imag(A1(2)));
C1 = 1/(w0*XC1);

% 1.2 OPERATING POINT #2
V2 = 2.0; % Operating point voltage #2 (V)
I2 = 20.0e-3; % Operating point current #2 (A)
s11_2 = -0.22505-j*0.3583171;
s12_2 = 0.02342899+j*0.035627;
s21_2 = -2.888729+j*14.419999;
s22_2 = 0.256483-j*0.373167;
A2 = S2ABCD(s11_2,s12_2,s21_2,s22_2,Z0);
XC2 = abs(imag(A2(2)));
C2 = 1/(w0*XC2);

% 1.2 OPERATING POINT #3
V3 = 3.0; % Operating point voltage #3 (V)
I3 = 10.0e-3; % Operating point current #3 (A)
s11_3 = -0.067625-j*0.537644;
s12_3 = 0.02910815+j*0.03888136;
s21_3 = -4.692475+j*11.902185;
s22_3 = 0.419550676-j*0.43626712;
A3 = S2ABCD(s11_3,s12_3,s21_3,s22_3,Z0);
XC3 = abs(imag(A3(2)));
C3 = 1/(w0*XC3);

% 1.2 OPERATING POINT #4
V4 = 3.0; % Operating point voltage #4 (V)
I4 = 20.0e-3; % Operating point current #4 (A)
```

```

s11_4 = -0.201618196-j*0.357915;
s12_4 = 0.020892921+j*0.034869877;
s21_4 = -3.171788+j*14.805157;
s22_4 = 0.29422055-j*0.37197621;
A4 = S2ABCD(s11_4,s12_4,s21_4,s22_4,Z0);
XC4 = abs(imag(A4(2)));
C4 = 1/(w0*XC4);

```

## SPICE Data Analysis Procedure (ANALYZE\_DATA.m)

```

clear
filename = 'pset005.txt';
Npts = 50000;
s = READVDATA(filename,Npts);
% s(1,:) = t s(2,:) = iL s(3,:) = vC2 s(4,:) = vC1
Npts = length(s(1,:));

dt = s(1,201)-s(1,200);
fmax = 1/dt;
f0 = 0.0;
df = (fmax-f0)/(Npts-1);
f = f0:df:fmax;
FvC1 = fft(s(4,:));

PSSD(1,1) = 0.0; % iL0
PSSD(2,1) = 1.2; % vC20
PSSD(3,1) = 1.0; % vC10
PSSD(1,2) = 0.08; % iLf
PSSD(2,2) = 2.5; % vC2f
PSSD(3,2) = 1.0; % vC1f
k = 0;
for m = 5000:Npts
    pssout = PSSCHK(s(2:4,m-1),s(2:4,m),PSSD);
    if pssout(1) == 1
        k = k + 1;
        ps(1,k) = pssout(2);
        ps(2,k) = pssout(3);
    end
end
if k > 0
    for i = 2:k
        rmpX(1,i-1) = ps(1,i-1); % iL return map X
        rmpX(2,i-1) = ps(1,i); % iL return map Y
        rmpY(1,i-1) = ps(2,i-1); % vC2 return map X
        rmpY(2,i-1) = ps(2,i); % vC2 return map Y
    end
    figure(1)
    plot(ps(1,:),ps(2,:),'.')
    xlabel('iL[n]')
    ylabel('vC2[n]')

    figure(2)

```

```
    plot(rmpY(1,:),rmpY(2,:),'.')
    xlabel('vC2[n]')
    ylabel('vC2[n+1]')
end
```

```
figure(3)
plot3(s(4,:),s(3,:),s(2,:))
xlabel('vC1');
ylabel('vC2');
zlabel('iL');
```

```
figure(4)
plot(f/1e6,abs(FvC1)/Npts)
xlabel('frequency (MHz)')
ylabel('Spectrum (V/Hz)')
axis([00 1000 0 0.15])
```



## APPENDIX B – SPICE Circuit Files

(All code is proprietary information and property of Syncrodyne Systems Corporation © 2002 All Rights

Reserved)

### 2 MHz Syncrodyne Amplifier Circuit

Created by TINA

```
*****  
** This file was created by TINA **  
** (c) 1996 DesignSoft, Inc. **  
*****
```

```
.LIB "TSPICE.LIB" ; for the examples only  
* Please use your own Spice libraries.
```

```
.TEMP 27
```

```
.AC DEC 16 1 1MEG
```

```
.TRAN 100N 50U UIC
```

```
.PROBE V(1) I(ViL) V(5) V(2)
```

```
ViL      3  4  ; AmperMeter
```

```
Vee      6  0  -3.2
```

```
Vcc      8  0  5
```

```
XRin     1  2  1  PotMeter PARAMS: Res=1 Percent=10M
```

```
XRe      6  2  6  PotMeter PARAMS: Res=189 Percent=10M
```

```
XP1      5  7  5  PotMeter PARAMS: Res=24.9 Percent=10M
```

```
L1       8  3  4.7U
```

```
CT       2  5  330P
```

```
Ce       0  2  1.8N
```

```
Cbase    2  5  1.5N
```

```
QT1      5  0  2  Q_2N3904_N
```

```
L2       4  7  2.2U
```

```
.MODEL Q_2N3904_N NPN( IS=9.99F NF=1 NR=1 RE=2.51 RC=1
```

```
+ RB=10 VAF=40 VAR=20 ISE=4.03P ISC=4.03P
```

```
+ ISS=0 NE=1.78 NC=1.78 NS=1 BF=679
```

```
+ BR=5 IKF=13.8M IKR=13.8M CJC=3.6P CJE=3.99P
```

```
+ CJS=0 VJC=878M VJE=16.1 VJS=750M MJC=307M
```

```
+ MJE=2.01 MJS=0 TF=531P TR=69N EG=1.11
```

```
+ KF=0 AF=1 )
```

```
.END
```

## 850 MHz Chaotic Oscillator with HBT

Created by TINA

```
*****  
** This file was created by TINA **  
** (c) 1996 DesignSoft, Inc. **  
*****
```

```
.LIB "TSPICE.LIB" ; for the examples only  
* Please use your own Spice libraries.  
.TEMP 27  
.AC DEC 16 1 1MEG  
.TRAN 2N 1U UIC
```

```
.PROBE I(ViL) V(3) V(2)
```

```
ViL      2    4    ; AmperMeter  
Vcc      5    0    10  
QT1      2    1    0    Q_HBT-SGA-83_N  
Rb       0    1    1.5K  
Cc       3    1    100P  
R1       5    2    150  
L        3    4    30N  
C1       2    0    10P  
C2       0    3    10P
```

```
.MODEL Q_HBT-SGA-83_N NPN(IS=9.99E-11 NF=0.701 NR=0.701 RE=106 RC=-  
55.2  
+ RB=4.25E3 VAF=90 VAR=45 ISE=2.82E-15 ISC=1E-10  
+ NE=0.744 NC=0.744 BF=179 BR=5 IKF=4.99E3  
+ IKR=4.99E3 CJC=3.3E-11 CJE=3E-11 VJC=1.99 VJE=0.75  
+ MJC=0.201 MJE=0.33 TF=7.96E-11 TR=5.48E-10 EG=1.11  
+ KF=0 AF=1)
```

```
.END
```

## LITERATURE CITED

1. T. Matsumoto, *A Chaotic Attractor from Chua's Circuit*, IEEE Trans. CAS-**31**, no. 12 (1984), 1055-1058.
2. L. Kocarev, K. S. Halle, K. Eckert, L. O. **Chua**, and U. Parlitz, *Experimental Demonstration of Secure Communications via Chaotic Synchronization*, International Journal of Bifurcations and **Chaos** in Applied Science and Technology, vol. 2, Sept., pp. 709-713, 1992.
3. S. Hayes, C. Grebogi, E. Ott, A. Mark, Phys. Rev. Lett. **73**, 1781 (1994).
4. John Sommerer, *The End of Classical Determinism*, Johns Hopkins APL Technical Digest, Vol. 16, No. 4, 1995.
5. Edward Ott, *Chaos in Dynamical Systems*, Cambridge Univ. Press, Canada, 1993.
6. James Gleick, *Chaos: Making a New Science*, Viking Penquin, Inc., New York, 1987.
7. Francis C. Moon, *Chaotic Vibrations: An Introduction for Applied Scientists and Engineers*, John Wiley & Sons, New York, 1987.
8. C. M. Glenn, S. Hayes, *Observation of Chaos in a Microwave Limiter Circuit*, IEEE Microwave and Guided Wave Letters, vol. 4, no. 12, December 1994.
9. S. Basu, S. A. Mass, T. Itoh, *Quasi-Periodic Route to Chaos in a Microwave Doubler*, IEEE Microwave and Guided Wave Letters, vol. 5, no. 7, July 1995.
10. Manfred Schroeder, *Fractals, Chaos, Power Laws: Minutes From and Infinite Paradise*, W.H. Freeman and Company, New York, 1991.
11. J.M.T. Thompson and H.B. Stewart, *Nonlinear Dynamics and Chaos*, John Wiley &

- Sons, LTD, New York, 1991.
12. L. M. Pecora and T. L. Carroll, *Synchronization in Chaotic Systems*, *Phys. Rev. Lett.* **64**, 821 (1990).
  13. T. Carroll, L. Pecora, et.al., *Nonlinear Dynamics in Circuits*, World Scientific Publishing Co. LTD, New Jersey, 1995.
  14. E. Ott, C. Grebogi, J. A. Yorke, *Phys. Rev. Lett.* **64**, 1196 (1990).
  15. S. Hayes, C. Grebogi, E. Ott, *Phys. Rev. Lett.* **70**, 3031 (1993).
  16. S. Hayes, C. Grebogi, E. Ott, A. Mark, *Phys. Rev. Lett.* **73**, 1781 (1994).
  17. Frost & Sullivan, *2001 World Handset RF-Semiconductor Markets*, January 2002.
  18. Frost & Sullivan, *Mobile Telecommunications Markets – 2<sup>nd</sup> Quarter 2001*, July 2001.
  19. S. M. Sze, *High-Speed Semiconductor Devices*, AT&T Bell Laboratories, John Wiley & Sons, New York, 1990.
  20. Robert Boylestad and Louis Nashelsky, *Electronic Devices and Circuit Theory*, Prentice Hall, Inc., New Jersey, 1992.
  21. Pierre Collet and Jean-Pierre Eckmann, *Iterated Maps on the Interval as Dynamical Systems*, Birkhauser, Boston, 1980.
  22. Scott T. Hayes, *A Segment-Hopping Source for Synthesizing Digitally Encoded Chaotic Signals*, *2001 Technology Digest*, Syncrodyne Systems Corporation, June 2001.
  23. Chance M. Glenn, *A Process for Synthesizing Bandlimited Chaotic Waveforms for Digital Signal Transmission*, *2001 Technology Digest*, Syncrodyne Systems Corporation, June 2001.

24. Theodore S. Rappaport, *Wireless Communications: Principles & Practice*, Prentice Hall, New Jersey, 1996.
25. Martin J. Hasler, *Electrical Circuits with Chaotic Behavior*, Proceedings of the IEEE, vol. 75, no. 8, August 1987.
26. Tim Sauer, James A. Yorke, and Martin Casdagli, *Embedology*, Journal of Statistical Physics **65** Nos. 3/4, 579–616 (November 1991).
27. Robert Hadaway, et. al., Applications of SiGe HBTs to Datacomm and Wireless, Excerpts from '98 Spring MRS meeting, Nortel Networks, 1999.

## VITA

Chance Glenn was born the last of eight children in Newark, New Jersey of parents Wallace and Shirley. He grew up in Dothan, Alabama and attended Dothan High School where his love for science fiction, drawing painting and creating, and tearing apart anything electrical was steered towards a college degree in electrical engineering.

Chance first attended Alabama A&M University in Huntsville, Alabama then transferred to the University of Maryland at College Park to finish his undergraduate work in electrical engineering in 1991. Along the way he met and married his wife Marsha and made his home in Columbia, Maryland. Chance and Marsha presently have four children: Michael, Markiss, Melyssa, and Morgen.

Chance received his Master's degree in Electrical Engineering from the Johns Hopkins University, Whiting School of Engineering in 1995 under the guidance of Dr. Charles Westgate. Dr. Westgate and colleague Dr. Christian Fazi encouraged Chance to enter the doctoral program at Johns Hopkins in 1997.

Professionally, Chance began his career in electrical engineering in 1986 by interning at the Harry Diamond Laboratory, which became the Army Research Laboratory. Soon he became a permanent employee there where he began to work in various areas of microwave research. His professional interaction with Dr. Scott Hayes led to an interest in chaotic dynamics and its application to engineering. He proceeded to author several papers and give numerous presentations in conferences both domestically and abroad.

In 1996 Chance left The Army Research laboratory to partner with Dr. Hayes in an entrepreneurial venture to apply chaotic dynamics to commercial applications. This

venture eventually led to the current company, Syncrodyne Systems Corporation, which Chance is co-founder with Dr. Hayes, president and majority shareholder. Syncrodyne Systems has been in operation since 1998 and has been awarded development contracts, raised venture capital, and gained revenues in its mission area. Syncrodyne currently has prototypes ready to be translated into commercial applications, and is entering into strategic partnerships with industry players.

Chance's intense interest in music has led him to form a publishing company, Morningbird Music, from which several of the songs he has written has been recorded to albums, received radio airplay, reached the top of music charts, received nominations from the Grammy Awards, the Dove Awards, and the National Association of Independent Music. He has been apart of performances at Merriweather Post Pavilion, Hylton Memorial Chapel, the National Mall in Washington, DC, and even sung before Congress. He is currently the worship ministry leader for Bridgeway Community Church in Columbia, Maryland, where many of his songs are used.